H1prelim-09-045
ZEUS-prel-09-011 Submitted to

XVII International Workshop on Deep Inelastic Scattering, DIS2009, April 26-30, 2009, Madrid
Parallel Session **Structure Functions**

Electronic Access: www-h1.desy.de/h1/www/publications/conf/conf_list.html

Combination and QCD Analysis of H1 and ZEUS Deep Inelastic $e^{\pm}p$ Scattering Cross Section Measurements

H1 and ZEUS Collaborations

Abstract

Deep inelastic scattering cross section measurements previously published by the H1 and ZEUS collaborations are combined taking into account correlations due to the systematic uncertainties. The combination is based on the complete set of HERA-I analyses. The combined data is used as the sole input for a next-to-leading order QCD parton distribution function fit. The resulting HERAPDFs have reduced uncertainties compared to separate analyses of the H1 and ZEUS experiments.

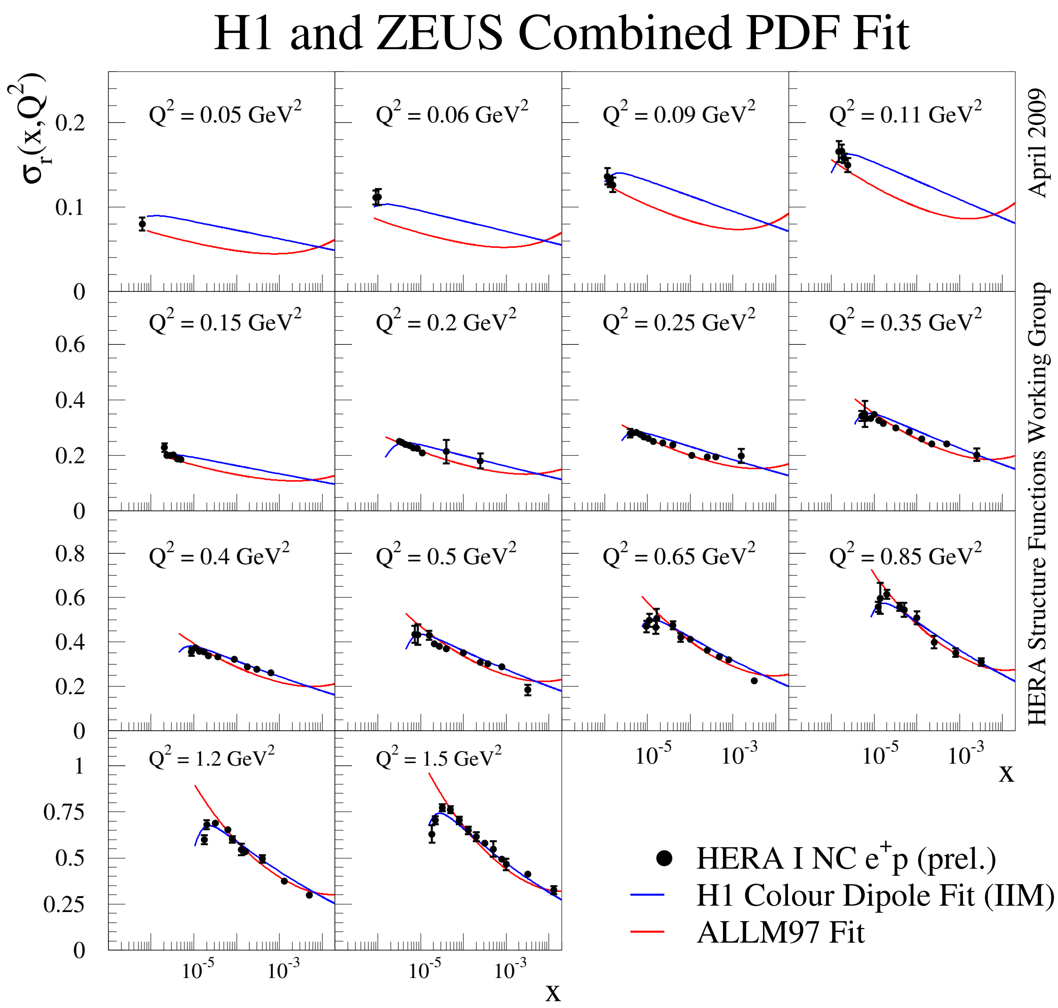

Figure 1: Figure shows the low Q^2 combined HERA I Neutral Current e^+p reduced cross section data (black filled circles) as function of x for various Q^2 bins in the range of $0.05 \geq Q^2 \geq 1.5$ GeV^2. This is the range of data which is not included in the QCD fit, therefore other models are considered. The curves represent fits based on various models, in red is the H1 Colour Dipole Model fit of IIM and in blue is the ALLM97 model fit.

H1 and ZEUS Combined PDF Fit

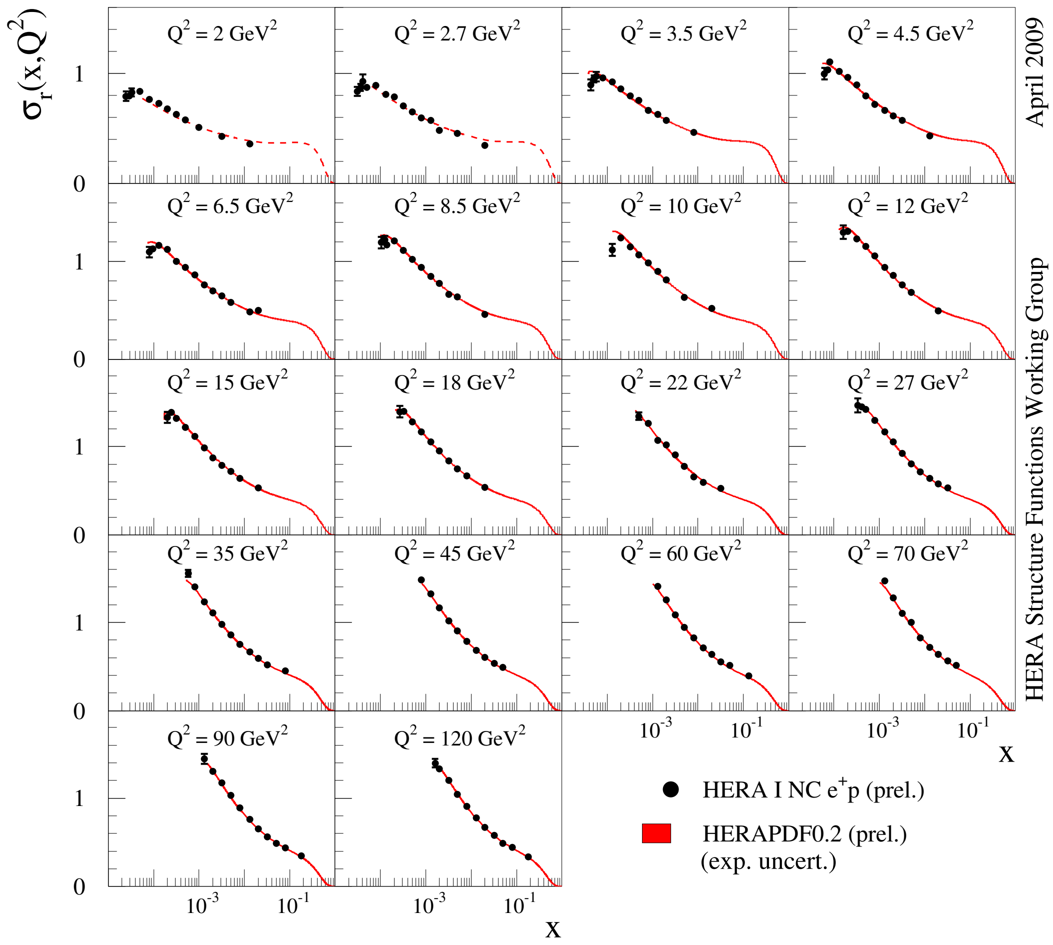

Figure 2: Figure shows the combined HERA I Neutral Current e^+p reduced cross section data (black filled circles) as function of x for various Q^2 bins in the region $120 \geq Q^2 \geq 2$ GeV^2 together with the HERAPDF0.2 fit. Both data and fit include the experimental errors.

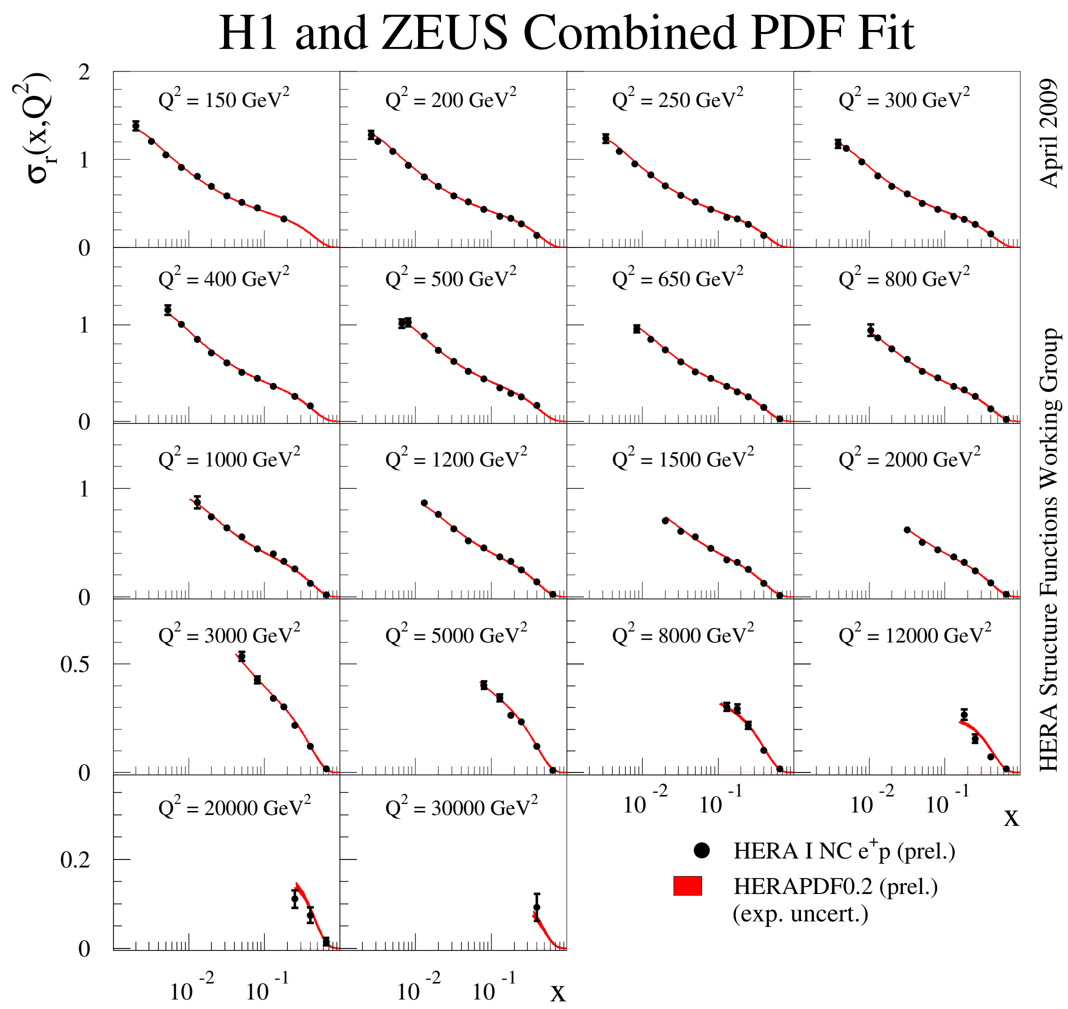

Figure 3: Figure shows the combined HERA I Neutral Current e^+p reduced cross section data (black filled circles) as function of x for various Q^2 bins in the region $30000 \geq Q^2 \geq 150$ GeV^2 together with the HERAPDF0.2 fit. Both data and fit include the experimental errors.

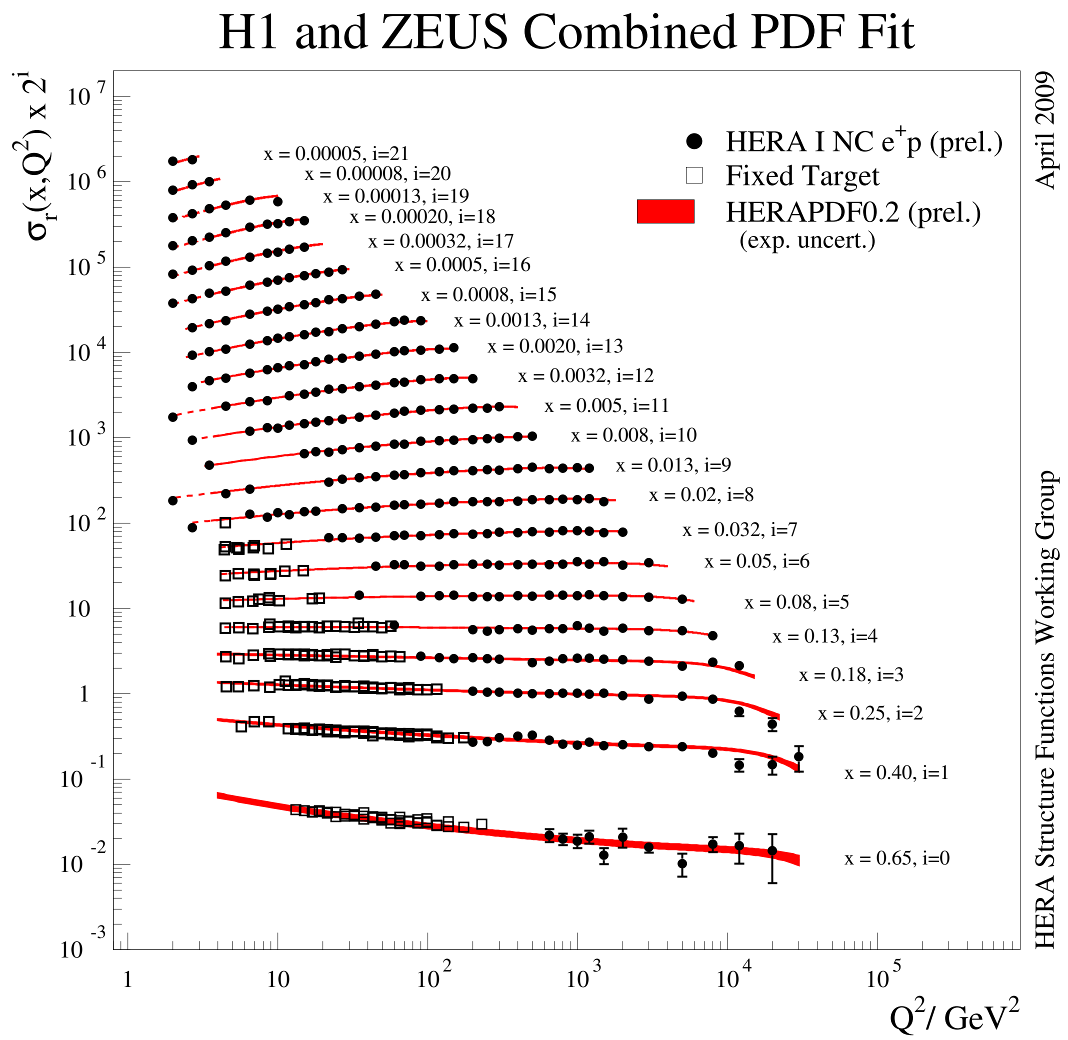

Figure 4: Figure shows the extended kinematic range of the HERA data (filled circles) as compared to the fixed target measurements (open squares). The red curve represents the fit corresponding to the complete inclusive HERA I data, the HERAPDF0.2. Both data and fit include the experimental errors. The scaling violations predicted by the theory of QCD are clearly observed.

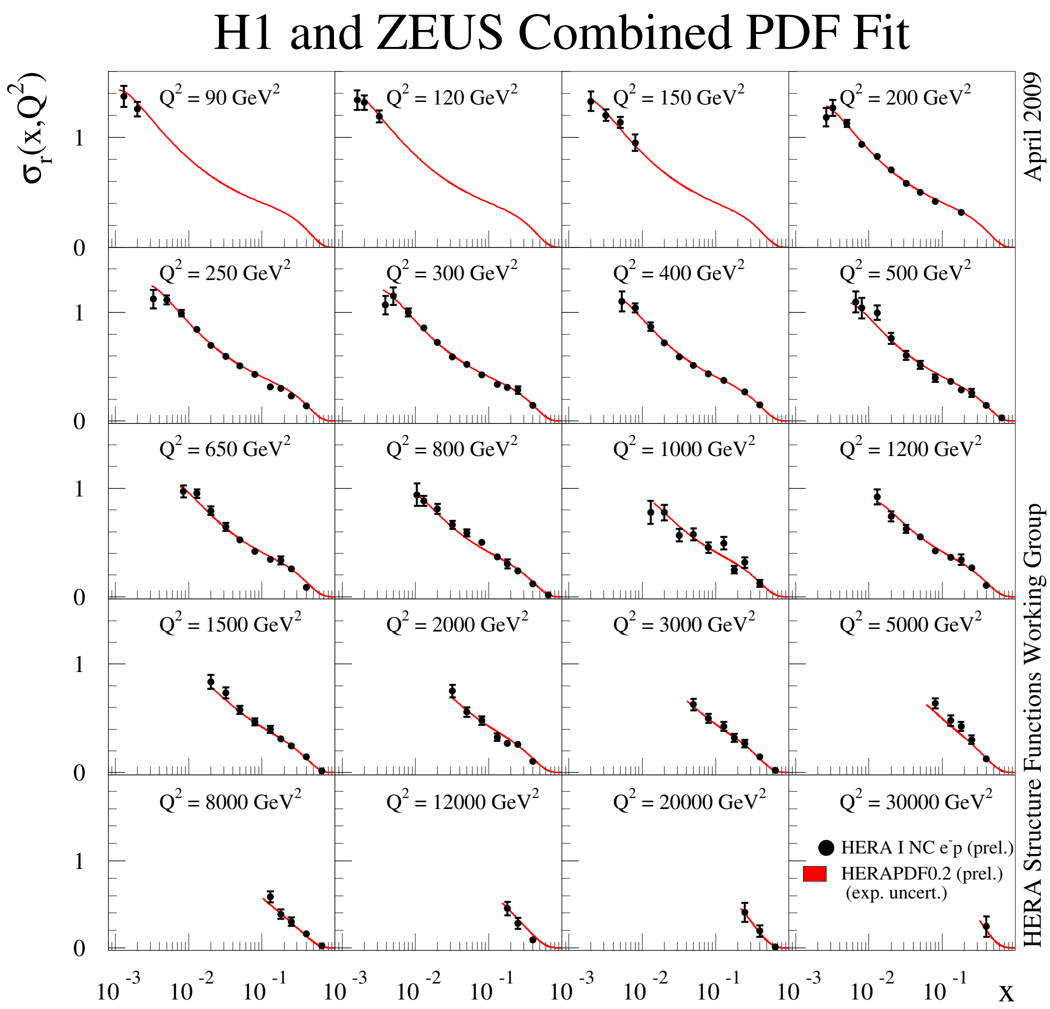

Figure 5: Figure shows the combined HERA I Neutral Current e^-p reduced cross section data (black filled circles) as function of x for various Q^2 bins in the region $30000 \geq Q^2 \geq 90$ GeV^2 together with the HERAPDF0.2 fit. Both data and fit include the experimental errors.

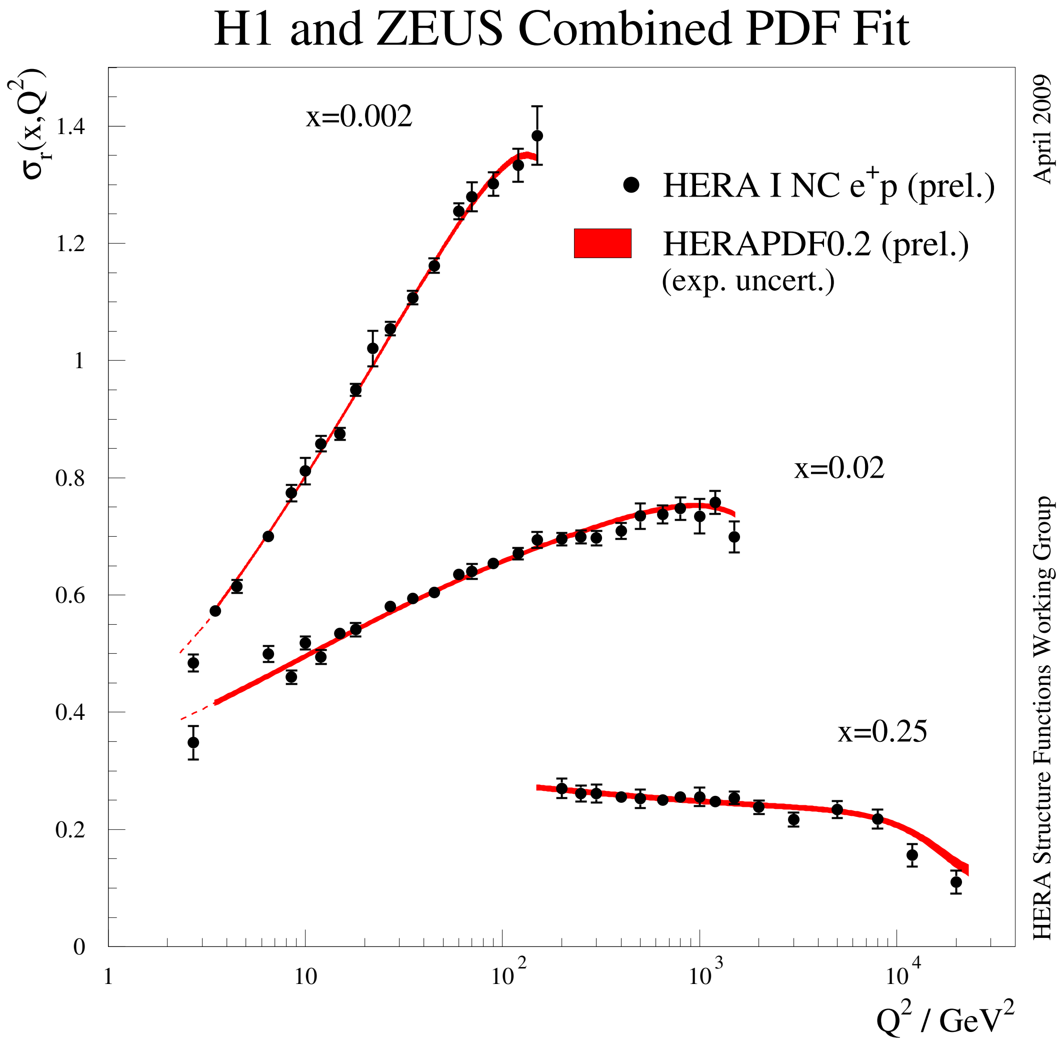

Figure 6: Figure shows in more details for selected x bins ($x = 0.002$, 0.02, 0.25) the averaged H1 and ZEUS NC e^+ reduced cross section measuerments (HERA I) as function of Q^2. The curve represents the fit corresponding to the complete inclusive HERA I data, the HERAPDF0.2, including the experimental errors. The scaling violations are clearly observed.

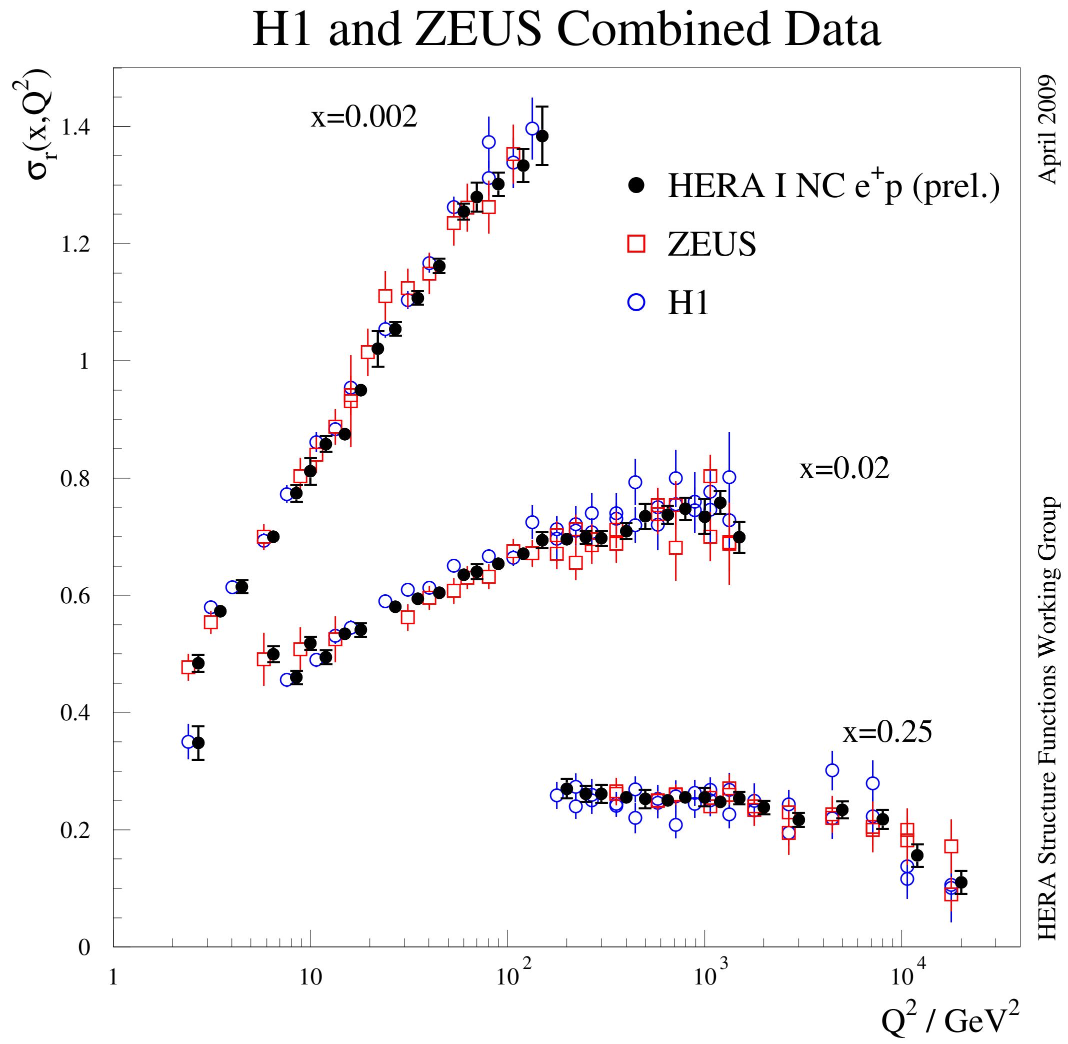

Figure 7: Figure shows in more details for selected x bins ($x = 0.002, 0.02, 0.25$) the NC e^+ reduced cross section measuerments (HERA I) as function of Q^2, before the averaging procedure (with open red squares ZEUS measurements alone, with open blue circles the H1 measurements alone) and after (with filled black circles). The error reductions after the averaging procedure are clearly observed.

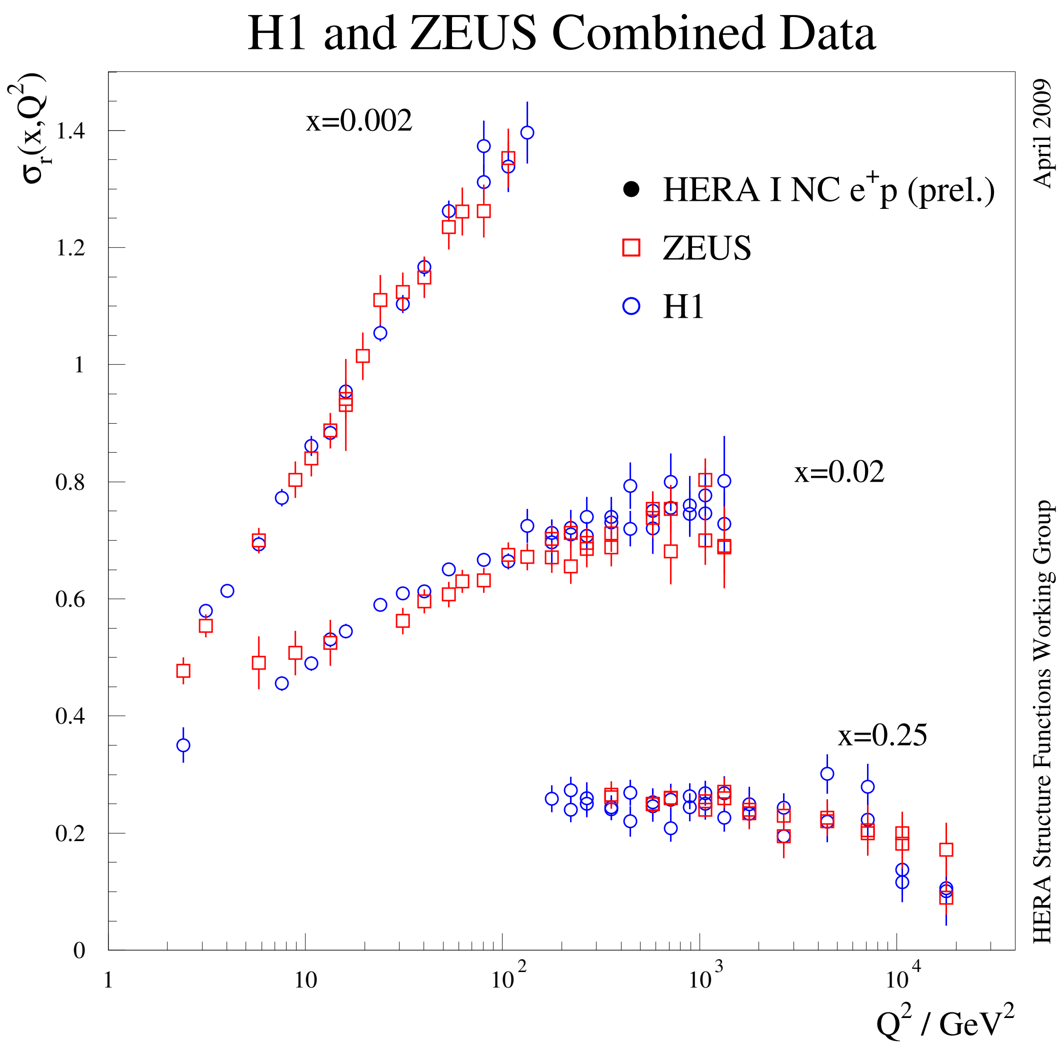

Figure 8: Figure shows in more details for selected x bins ($x = 0.002, 0.02, 0.25$) the NC e^+ reduced cross section measuerments (HERA I) as function of Q^2 before the averaging procedure (with open red squares ZEUS measurements alone, with open blue circles the H1 measurements alone).

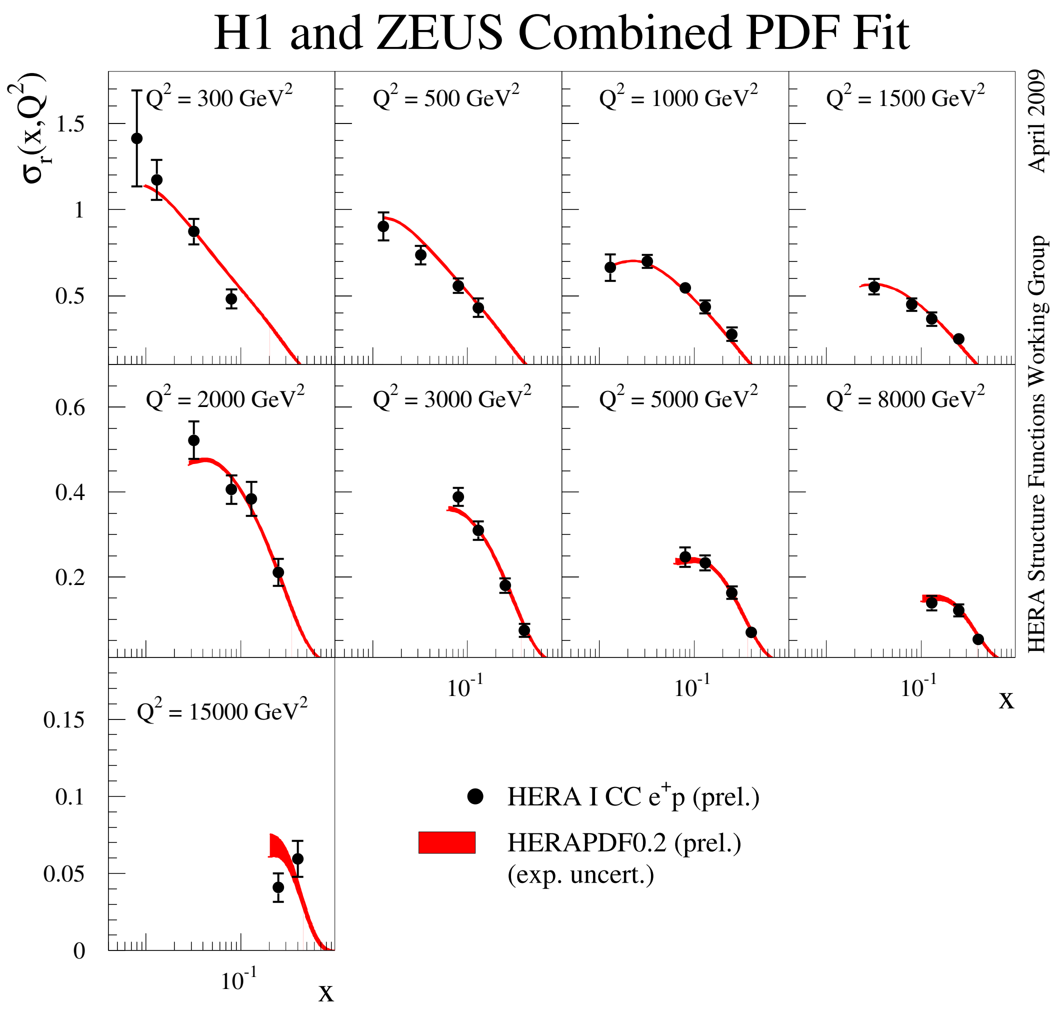

Figure 9: Figure shows the combined HERA I Charged Current e^+p reduced cross section data (black filled circles) as function of x for various Q^2 bins in the region $15000 \geq Q^2 \geq 300$ GeV^2 together with the HERAPDF0.2 fit. Both data and fit include the experimental errors.

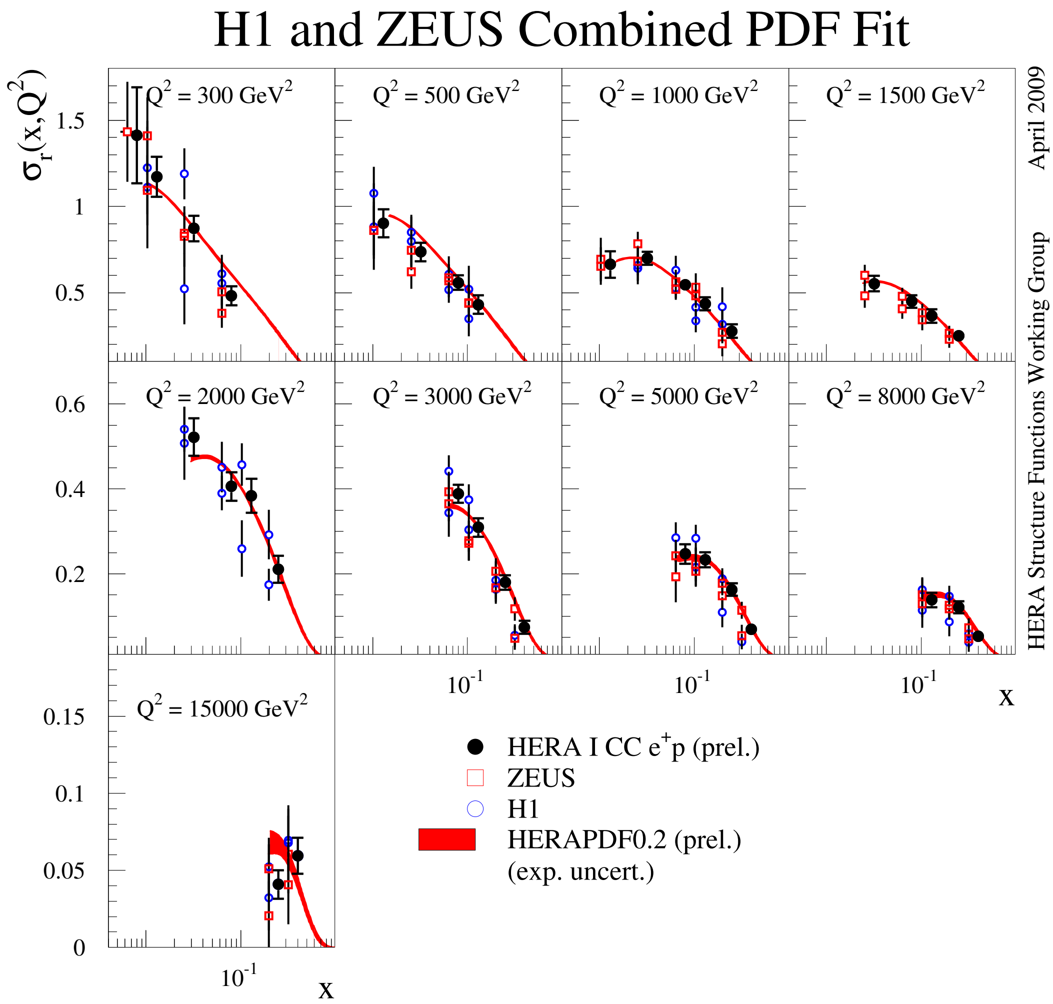

Figure 10: Figure shows the Charged Current e^+p reduced cross section data before the averaging procedure (with red open squares the ZEUS measurements alone, with blue open circles the H1 measurements alone) and after (black filled circles) as function of x for various Q^2 bins in the region $15000 \geq Q^2 \geq 300$ GeV^2. The curve is the HERAPDF0.2 fit. Both data and fit include the experimental errors. The reduction of the errors after the combination of the data is clearly observed.

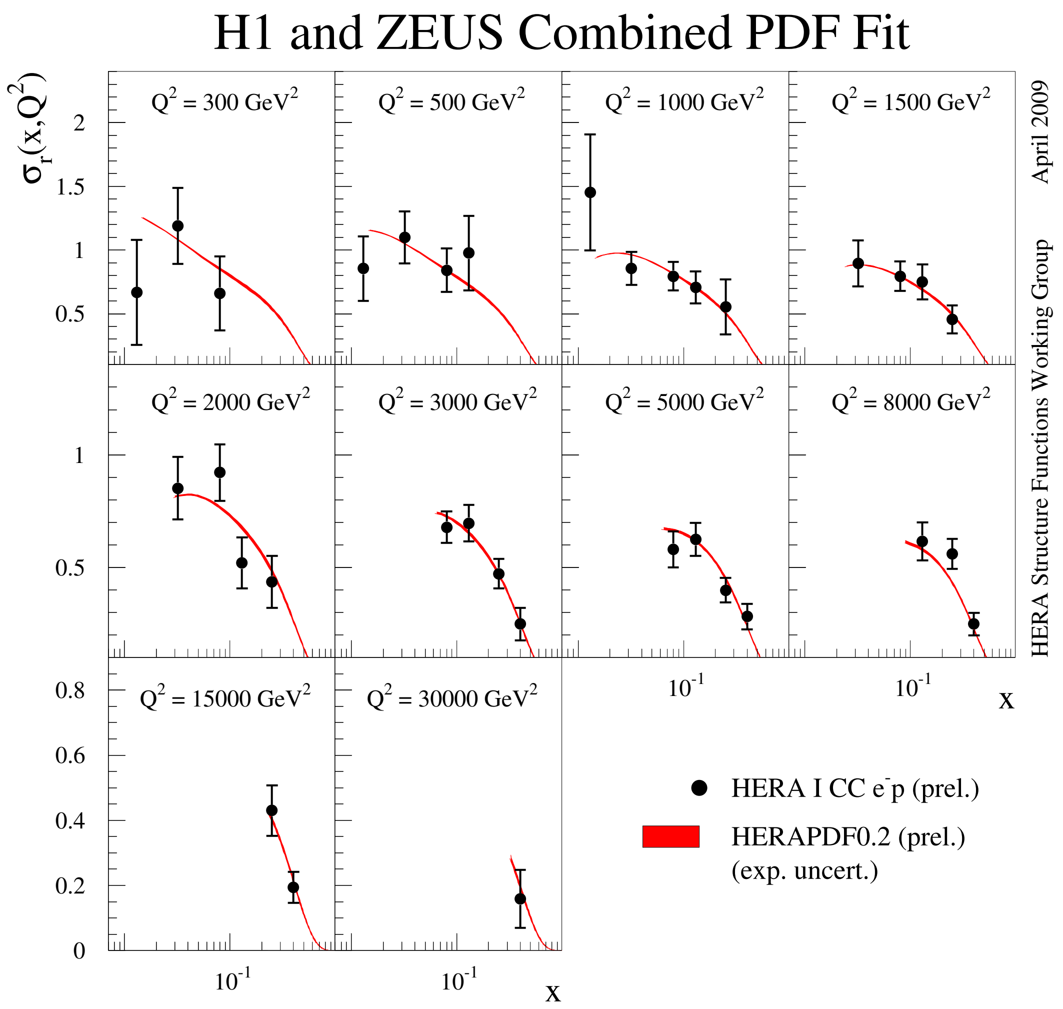

Figure 11: Figure shows the combined HERA I Charged Current e^-p reduced cross section data (black filled circles) as function of x for various Q^2 bins in the region $15000 \geq Q^2 \geq 300$ GeV^2 together with the HERAPDF0.2 fit. Both data and fit include the experimental errors.

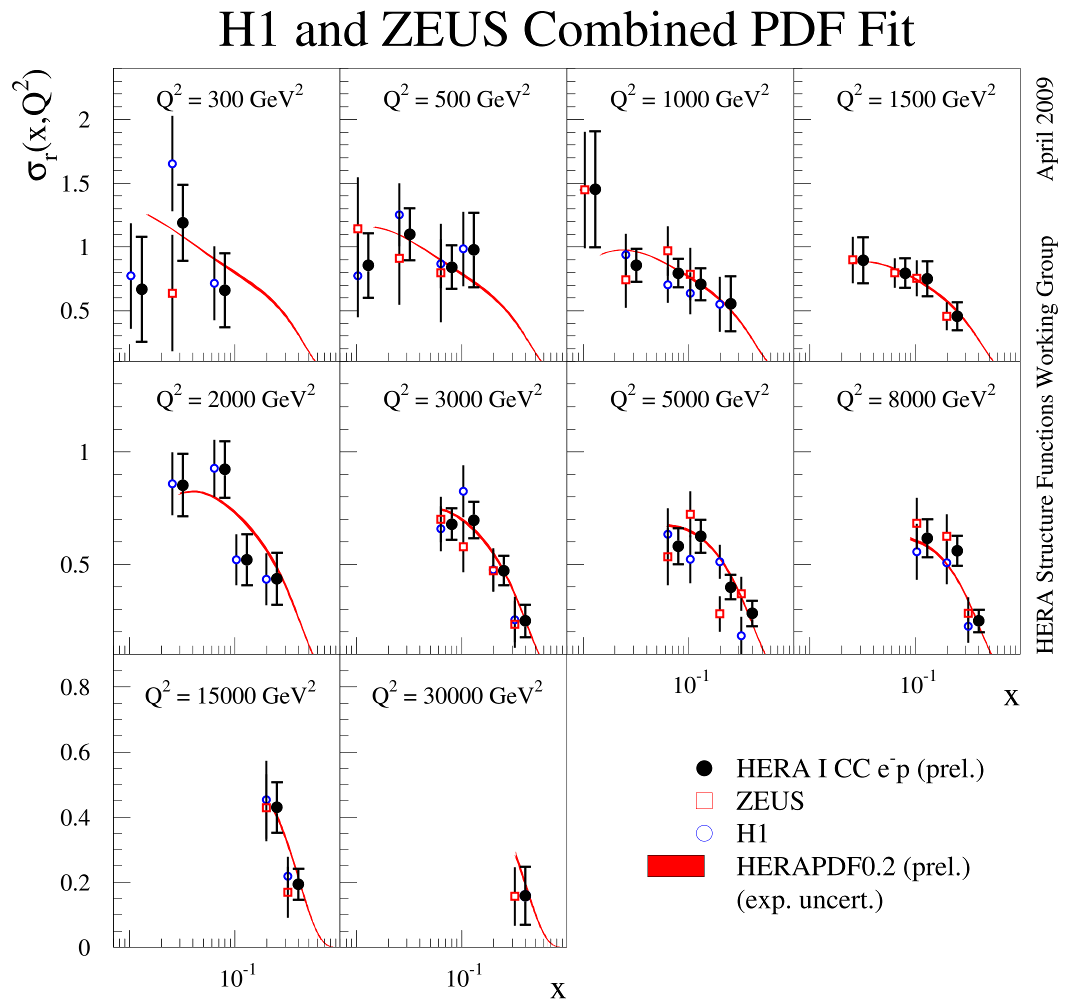

Figure 12: Figure shows the Charged Current e^-p reduced cross section data before the averaging procedure (with red open squares the ZEUS measurements alone, with blue open circles the H1 measurements alone) and after (black filled circles) as function of x for various Q^2 bins in the region $15000 \geq Q^2 \geq 300$ GeV^2. The curve is the HERAPDF0.2 fit. Both data and fit include the experimental errors. The reduction of the errors after the combination of the data is clearly observed.

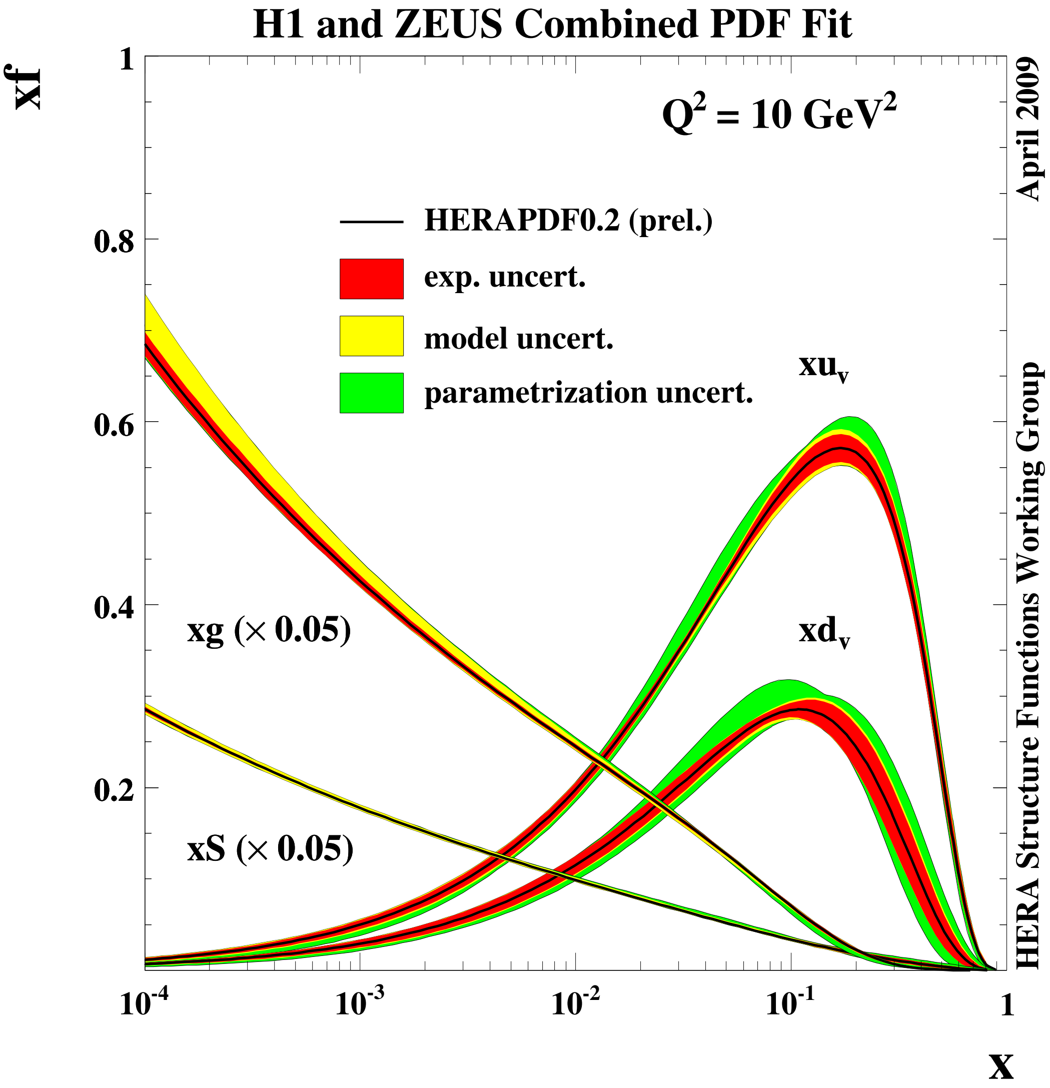

Figure 13: Figure shows the summary plot for the HERAPDF0.2 at the $Q^2 = 10$ GeV^2. The shown PDFs are the gluon, sea (which are scaled to better view) and the valence distributions. The errors include the experimental (red), model (yellow) and the PDF parametrisation (green) uncertainties. The PDF parametrisation dominates the high x region and the valence distributions.

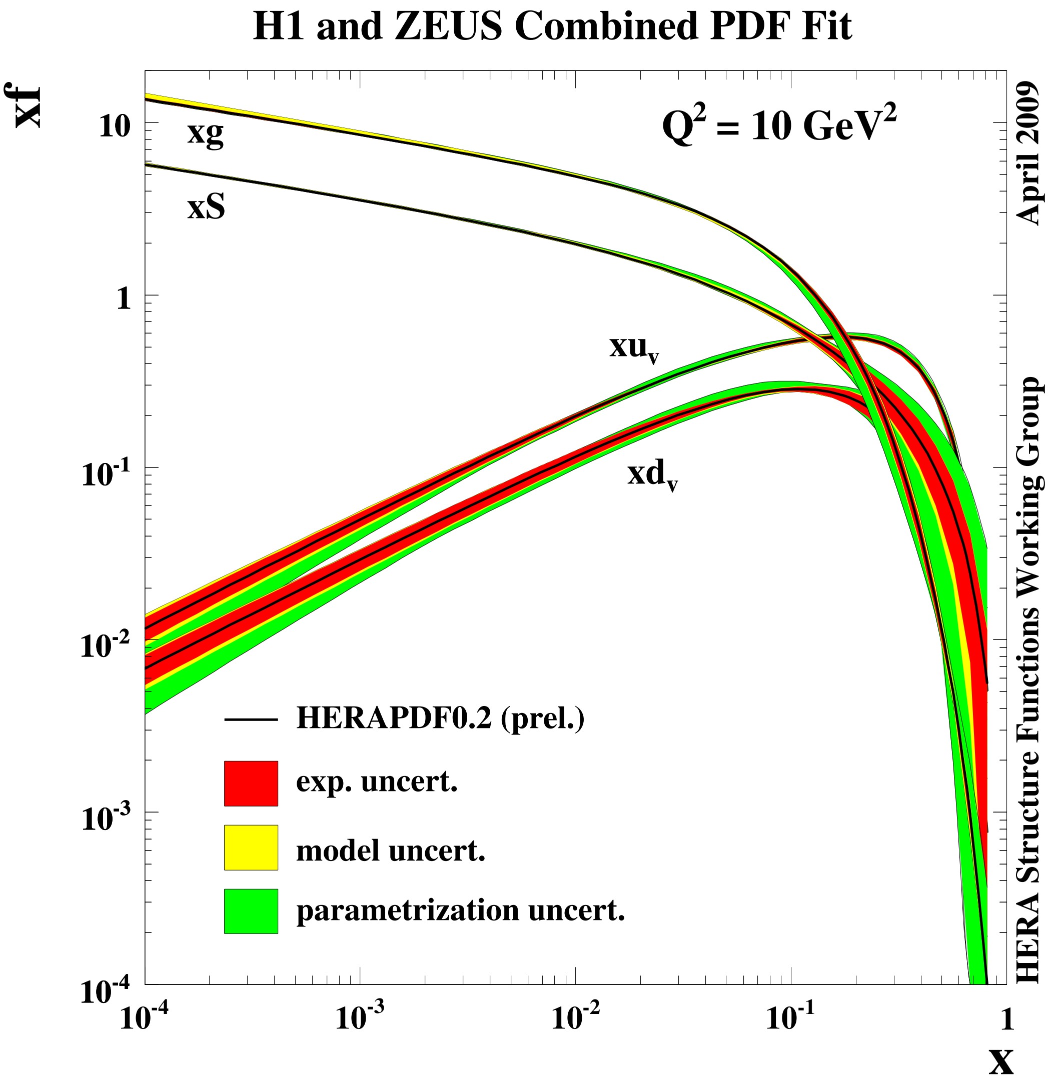

Figure 14: Figure shows the summary plot for the HERAPDF0.2 at the $Q^2 = 10$ GeV^2 in the logarithmic scale, so that there is no need to scale the distributions. The shown PDFs are the gluon, sea and the valence distributions. The errors include the experimental (red), model (yellow) and the PDF parametrisation (green) uncertainties. The PDF parametrisation dominates the high x region and the valence distributions.

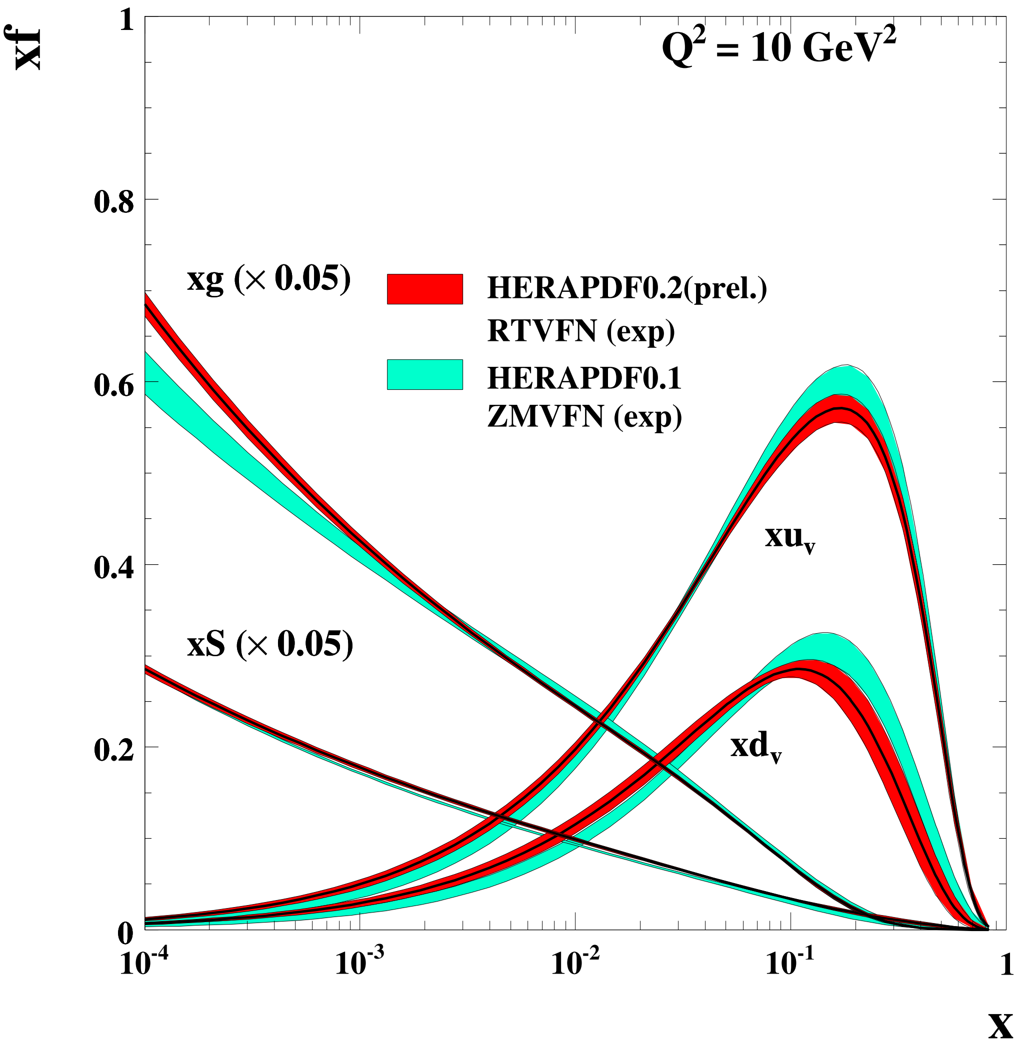

Figure 15: Figure shows a summary plot for direct comparison between the HERAPDF0.1 (cyan) and HERAPDF0.2 (red) at the $Q^2 = 10$ GeV^2. Only the experimental errors are used for this display, since there are differences in the evaluation of the model uncertainties and HERAPDF0.1 did not evaluate the PDF parametrisation uncertainties. Experimental errors are clearly improved with the inclusion of the more precise low Q^2 data for the HERAPDF0.2. The differences in the gluon shapes are mainly attributed to the improved theoretical model used for the extraction of the HERAPDF0.2 which used the non-zero mass for the quarks within the Roberts and Thorne Variable Flavour Number of schemes (RTVFN), as opposed to the Zero Mass Variable Flavour Number of schemes (ZMVFN) used for the HERAPDF0.1. Also, the starting scale used to extract the HERAPDF0.2 is $Q_0^2 = 1.9$ GeV^2, as opposed to 4 GeV^2 used for the HERAPDF0.1, as well as a more simplified χ^2 definition.

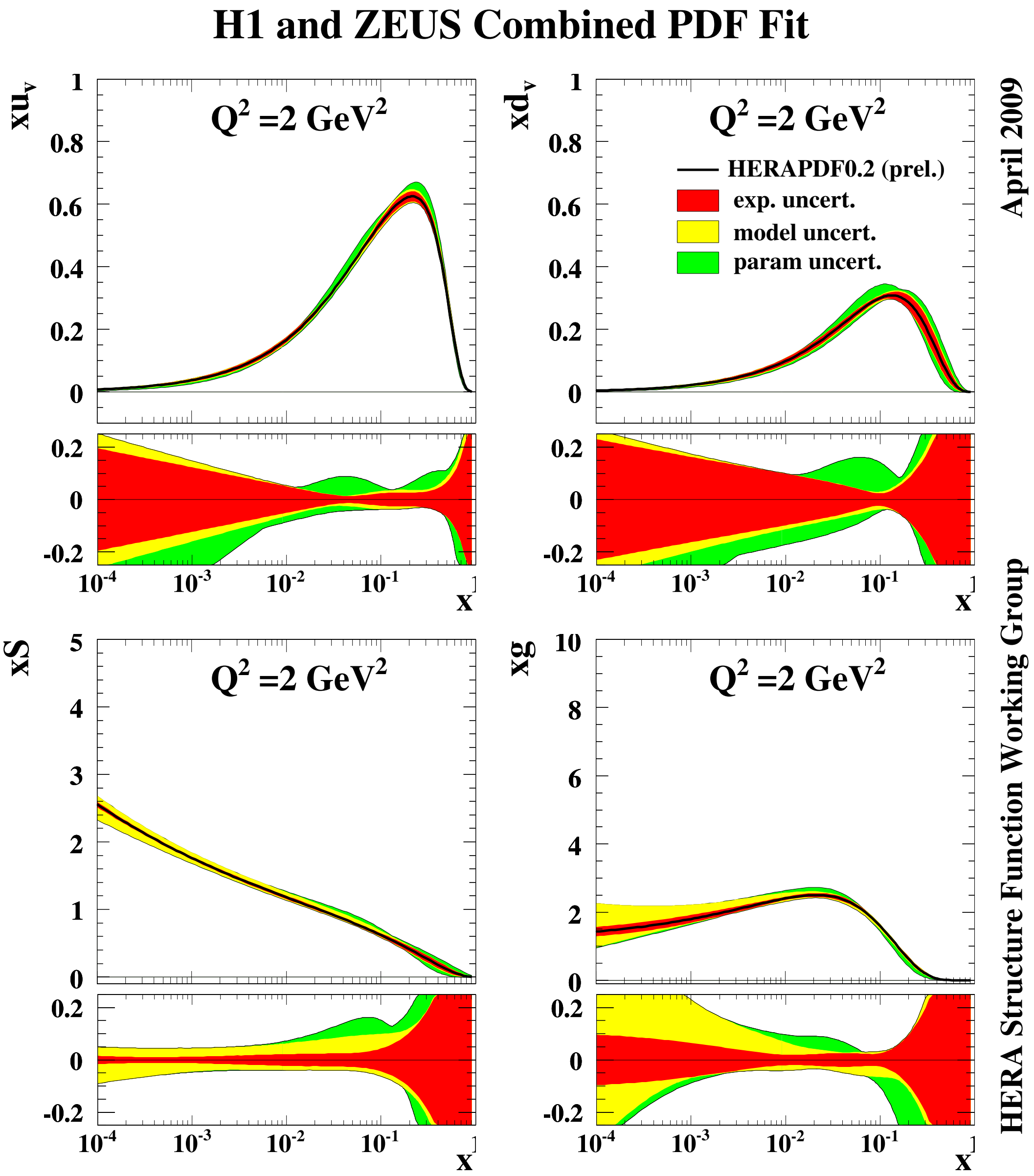

Figure 16: Figure shows the PDF distributions for the xu_v, xd_v, xS, and xg and their relative uncertainties which include the experimental (red), model (yellow), and parametrisation (green) uncertainties at the $Q^2 = 2$ GeV^2, near the starting scale. The shape of the gluon distribution is valence like. The HERAPDF0.2 errors of the sea and gluon distributions in the low x region are dominated by the model uncertainties, the largest of which are due to the variations in the starting scale Q_0^2 . The valence distributions are dominated by the parametrisation uncertainties and at high x this unceratinty dominates all the distributions.

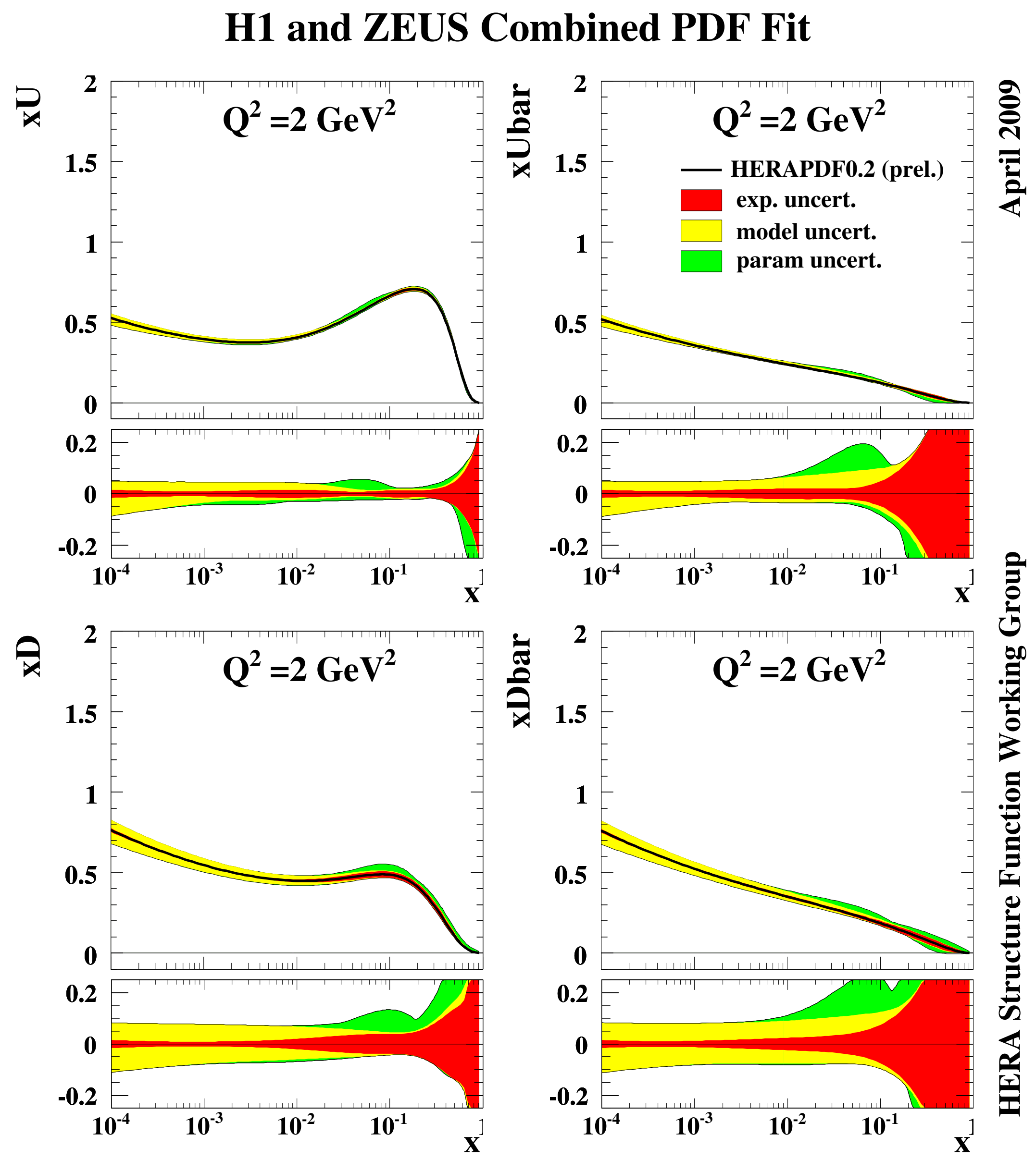

Figure 17: Figure shows the PDF distributions for the xU, $x\bar{U}$, xD, and $x\bar{D}$ and their relative uncertainties which include the experimental (red), model (yellow), and parametrisation (green) uncertainties at the $Q^2 = 2$ GeV^2, near the starting scale. The HERAPDF0.2 in the low x region are dominated by the model uncertainties. At medium and high x the parametrisation uncertainty dominates.

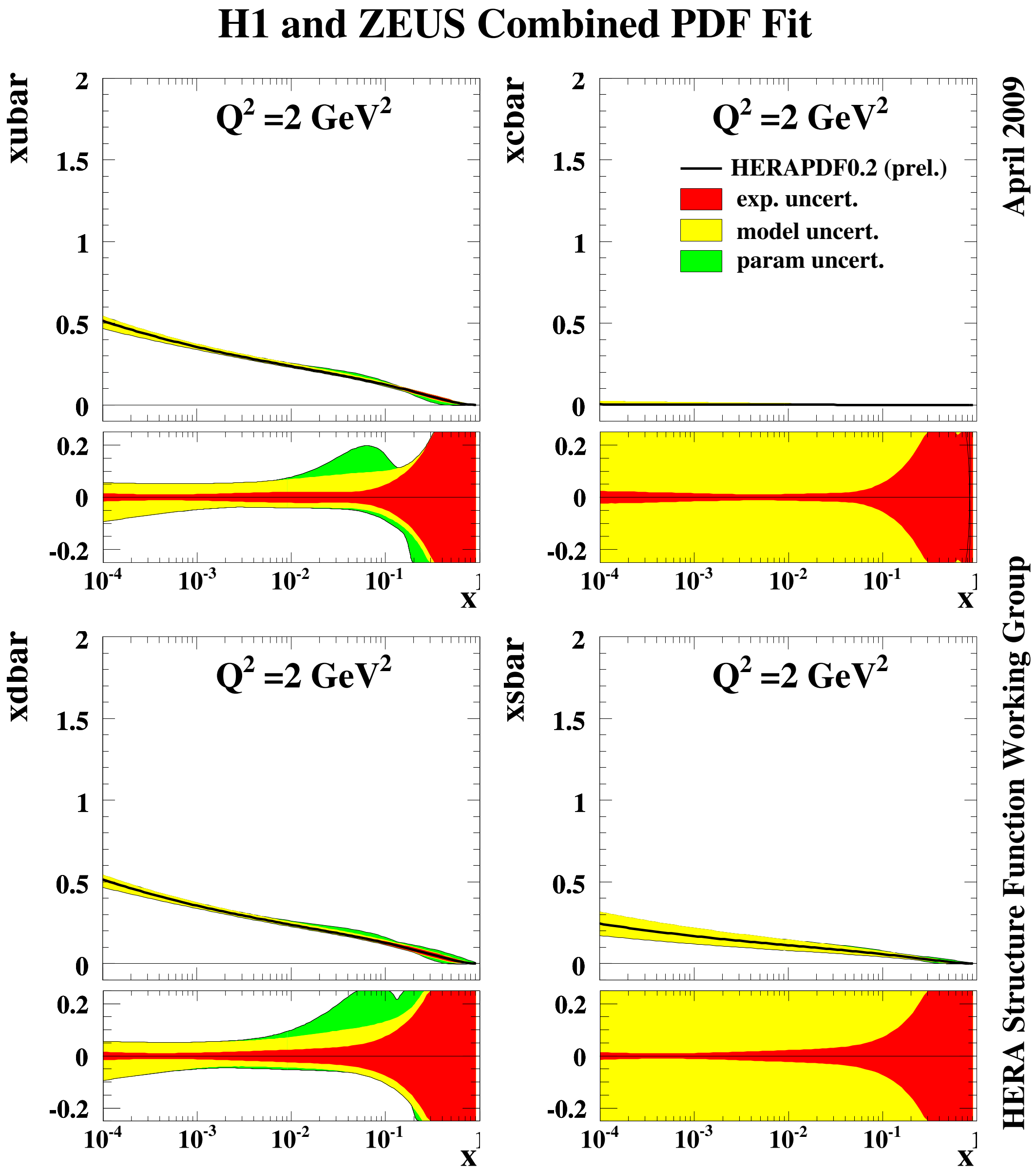

Figure 18: Figure shows the PDF distributions for the $x\bar{u}$, $x\bar{c}$, $x\bar{d}$, and $x\bar{s}$ and their relative uncertainties which include the experimental (red), model (yellow), and parametrisation (green) uncertainties at the $Q^2 = 2$ GeV^2, near the starting scale. The dominant error for the $x\bar{c}$ distribution is due to the uncertainty on the fraction of the charm in the sea, and similarly for the $x\bar{s}$ is the fraction of the strange in the sea dominates. At high x the parametrisation unceratinty dominates.

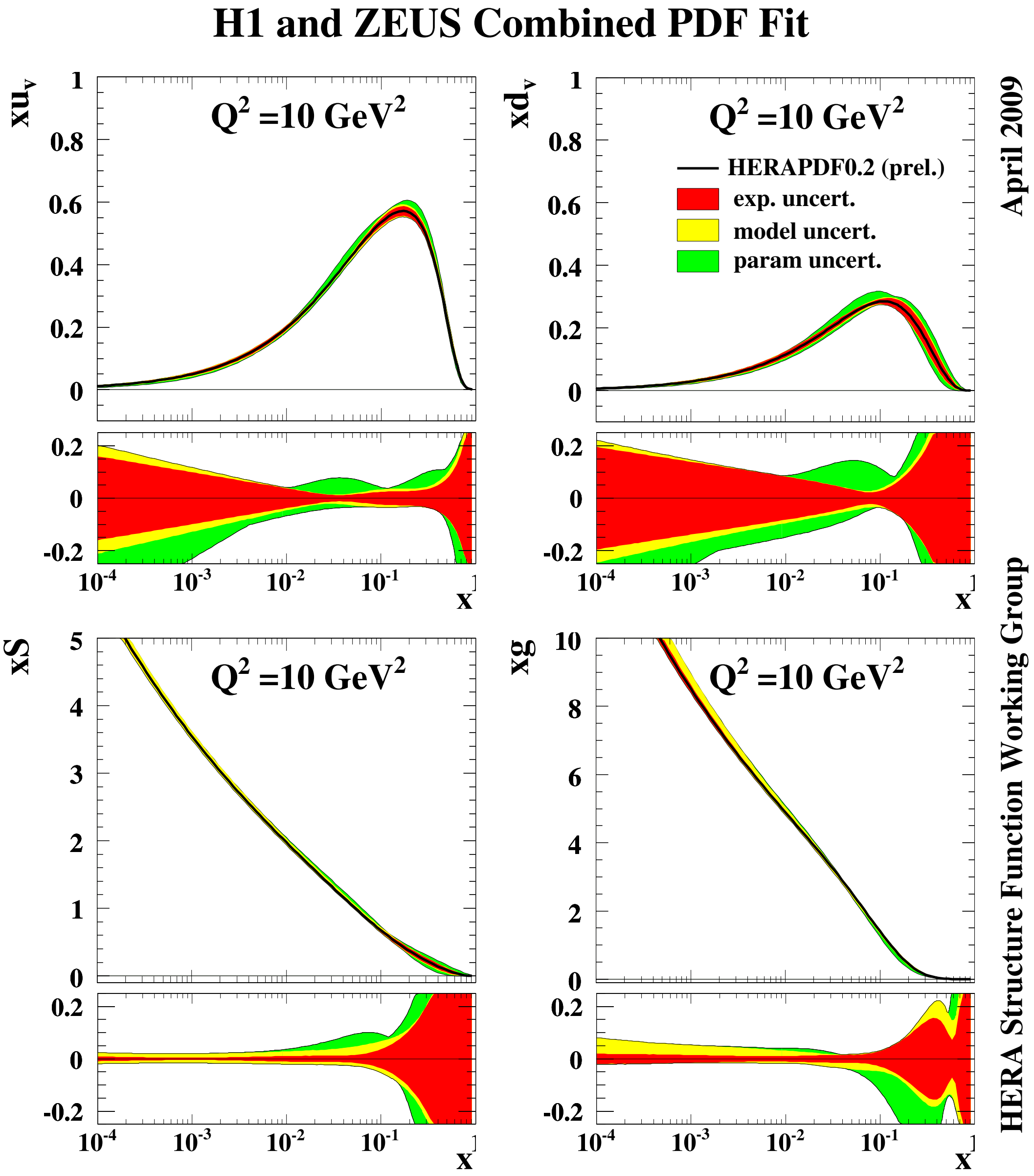

Figure 19: Figure shows the PDF distributions for the xu_v, xd_v, xS, and xg and their relative uncertainties which include the experimental (red), model (yellow), and parametrisation (green) uncertainties at the $Q^2 = 10$ GeV^2. The HERAPDF0.2 errors of the sea and gluon distributions in the low x region have an impresive precision. The valence distributions are dominated by the parametrisation uncertainties and at high x this unceratinty dominates all the distributions.

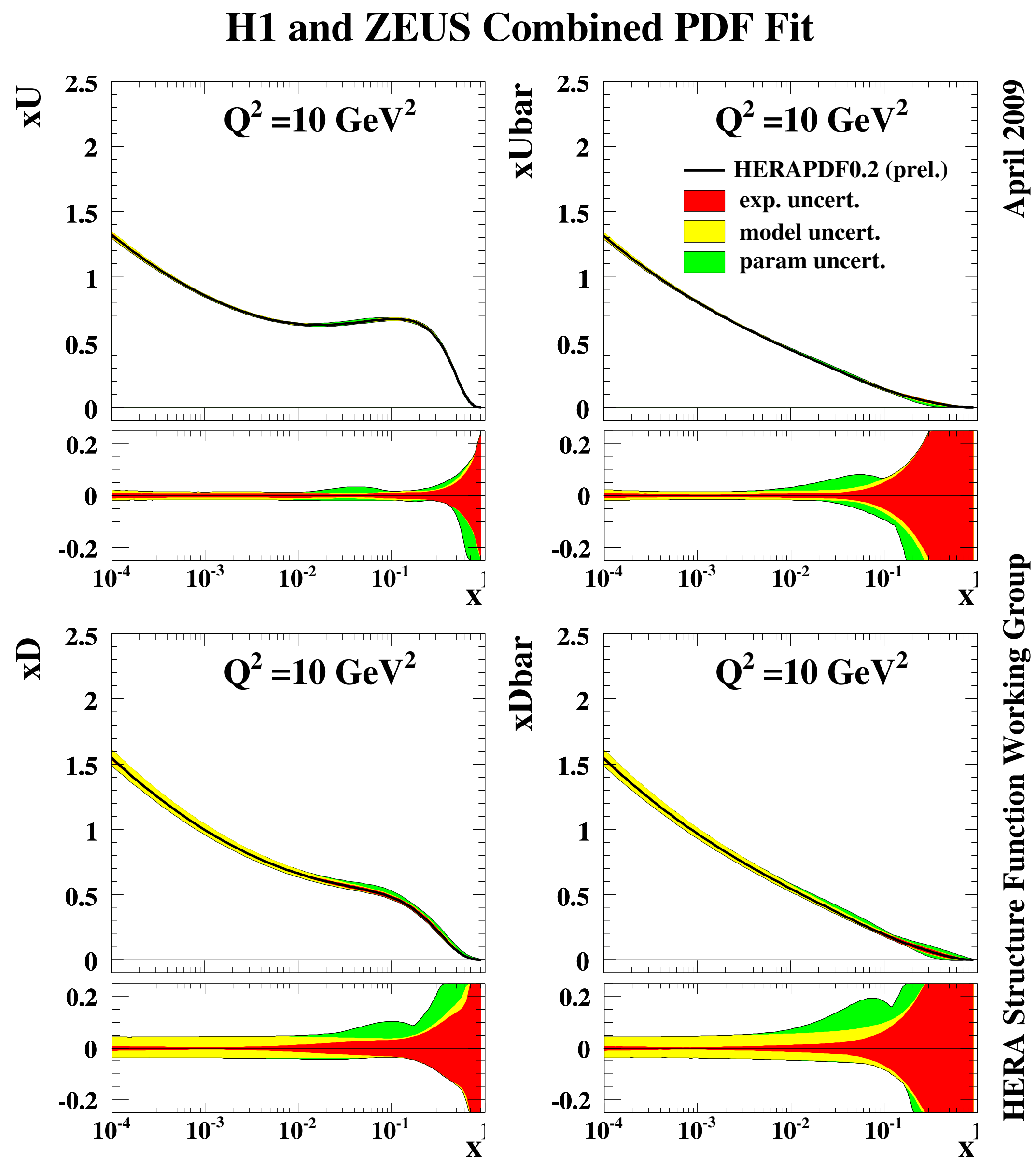

Figure 20: Figure shows the PDF distributions for the xU, $x\bar{U}$, xD, and $x\bar{D}$ and their relative uncertainties which include the experimental (red), model (yellow), and parametrisation (green) uncertainties at the $Q^2 = 10$ GeV^2. The HERAPDF0.2 errors at this scale are impressive, especially in the low x region. At high x the parametrisation uncueratinty dominates.

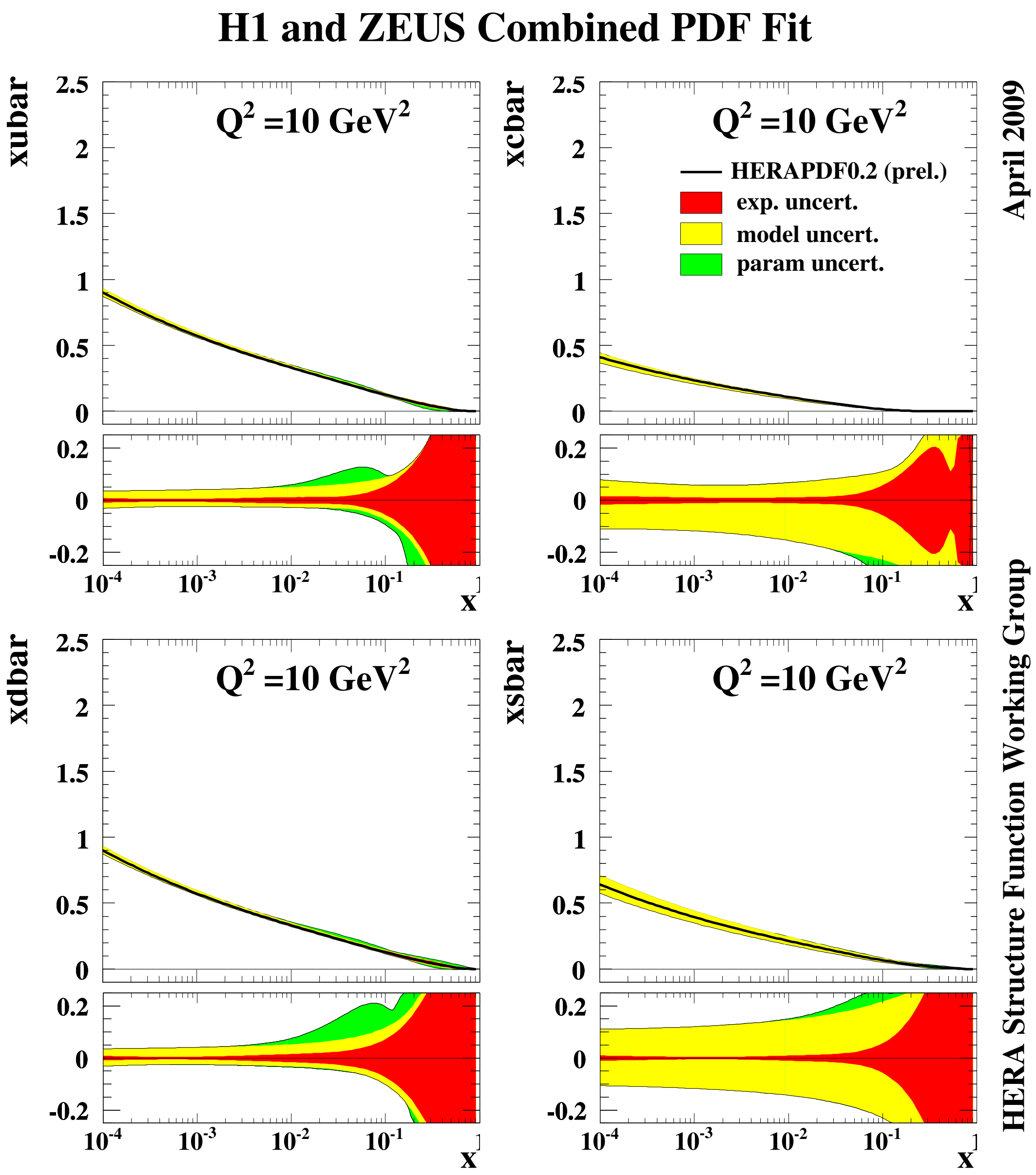

Figure 21: Figure shows the PDF distributions for the $x\bar{u}$, $x\bar{c}$, $x\bar{d}$, and $x\bar{s}$ and their relative uncertainties which include the experimental (red), model (yellow), and parametrisation (green) uncertainties at the $Q^2 = 10$ GeV^2. The HERAPDF0.2 errors at this scale are impressive, especially in the low x region. At high x the parametrisation uceratinty dominates.

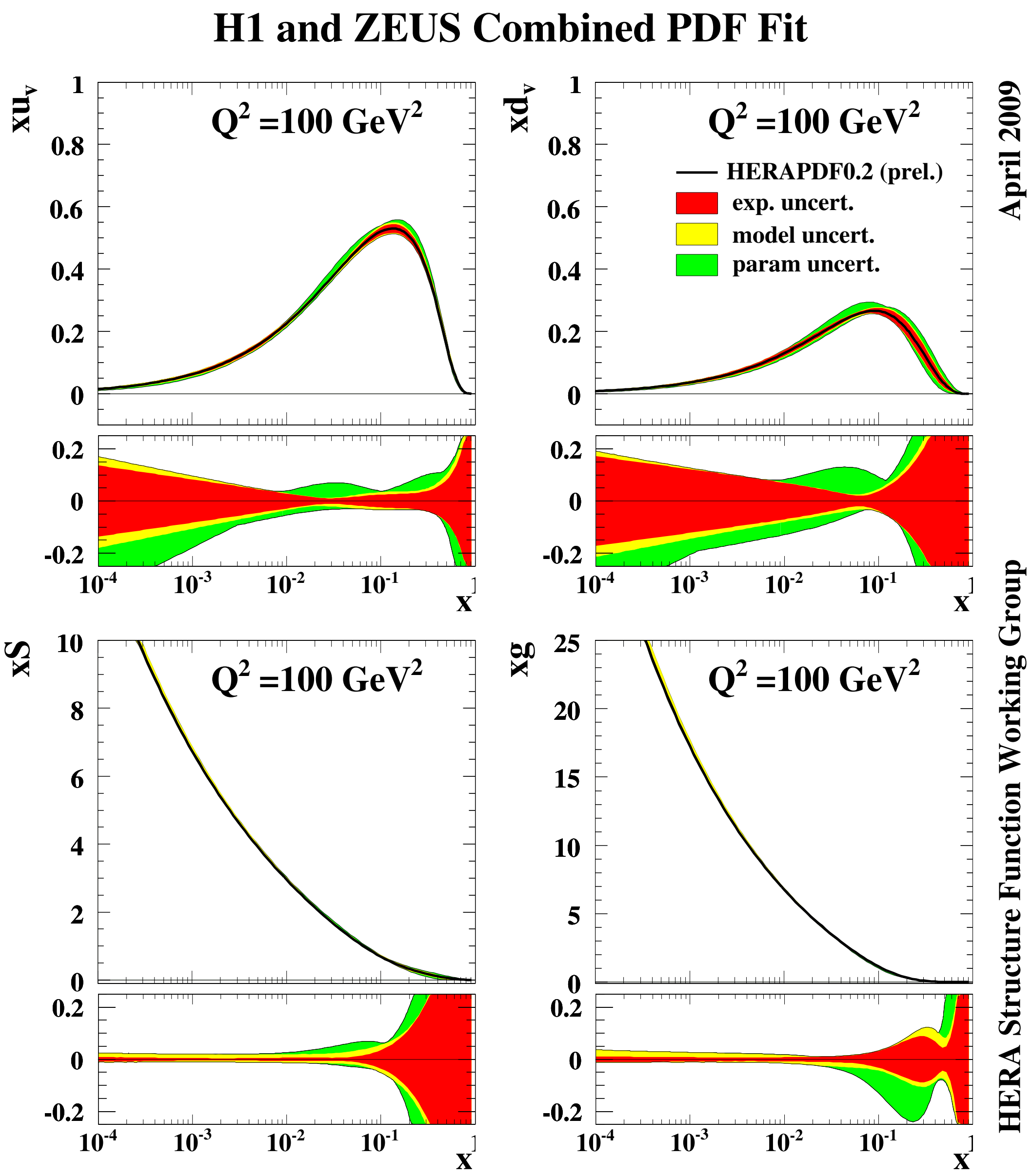

Figure 22: Figure shows the PDF distributions for the xu_v, xd_v, xS, and xg and their relative uncertainties which include the experimental (red), model (yellow), and parametrisation (green) uncertainties at the $Q^2 = 100\,\mathrm{GeV}^2$. The HERAPDF0.2 errors of the sea and gluon distributions in the low x region have an impresive precision. The valence distributions are dominated by the parametrisation uncertainties and at high x this unceratinty dominates all the distributions.

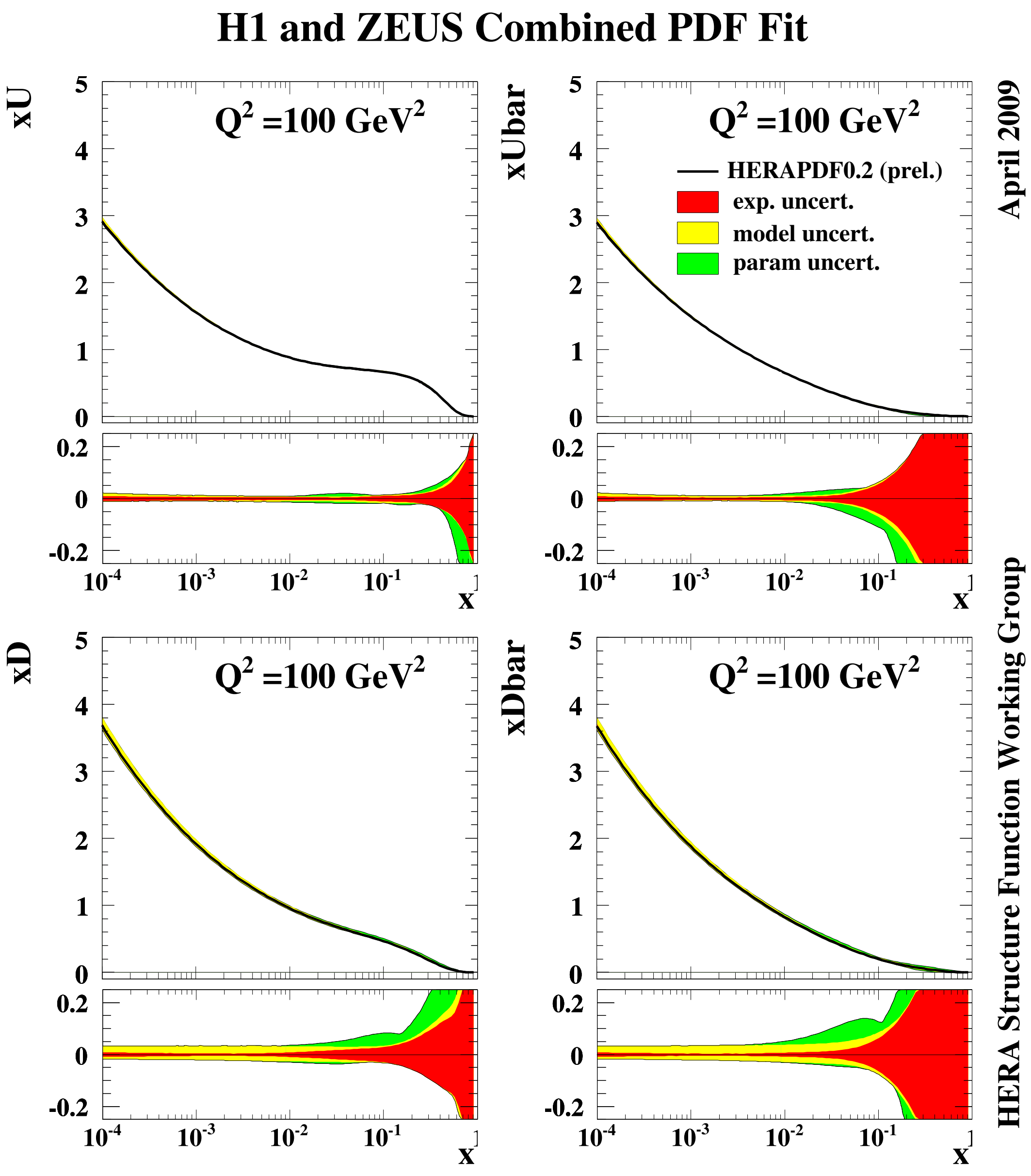

Figure 23: Figure shows the PDF distributions for the xU, $x\bar{U}$, xD, and $x\bar{D}$ and their relative uncertainties which include the experimental (red), model (yellow), and parametrisation (green) uncertainties at the $Q^2 = 100$ GeV^2. The HERAPDF0.2 errors at this scale are impressive, especially in the low x region. At high x the parametrisation uncertainty dominates.

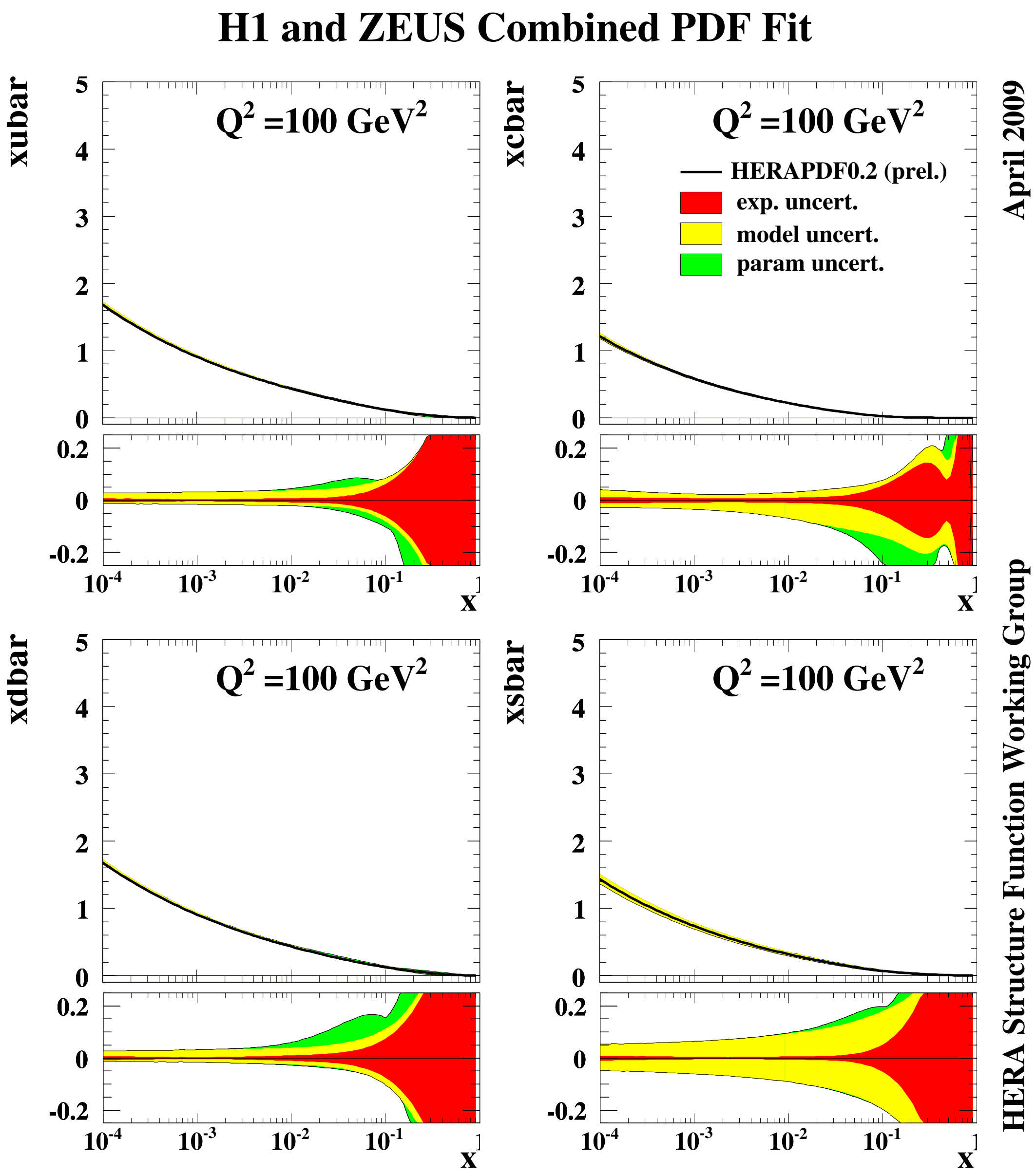

Figure 24: Figure shows the PDF distributions for the $x\bar{u}$, $x\bar{c}$, $x\bar{d}$, and $x\bar{s}$ and their relative uncertainties which include the experimental (red), model (yellow), and parametrisation (green) uncertainties at the $Q^2 = 100$ GeV^2. The HERAPDF0.2 errors at this scale are impressive, especially in the low x region. At high x the parametrisation uncertainty dominates.

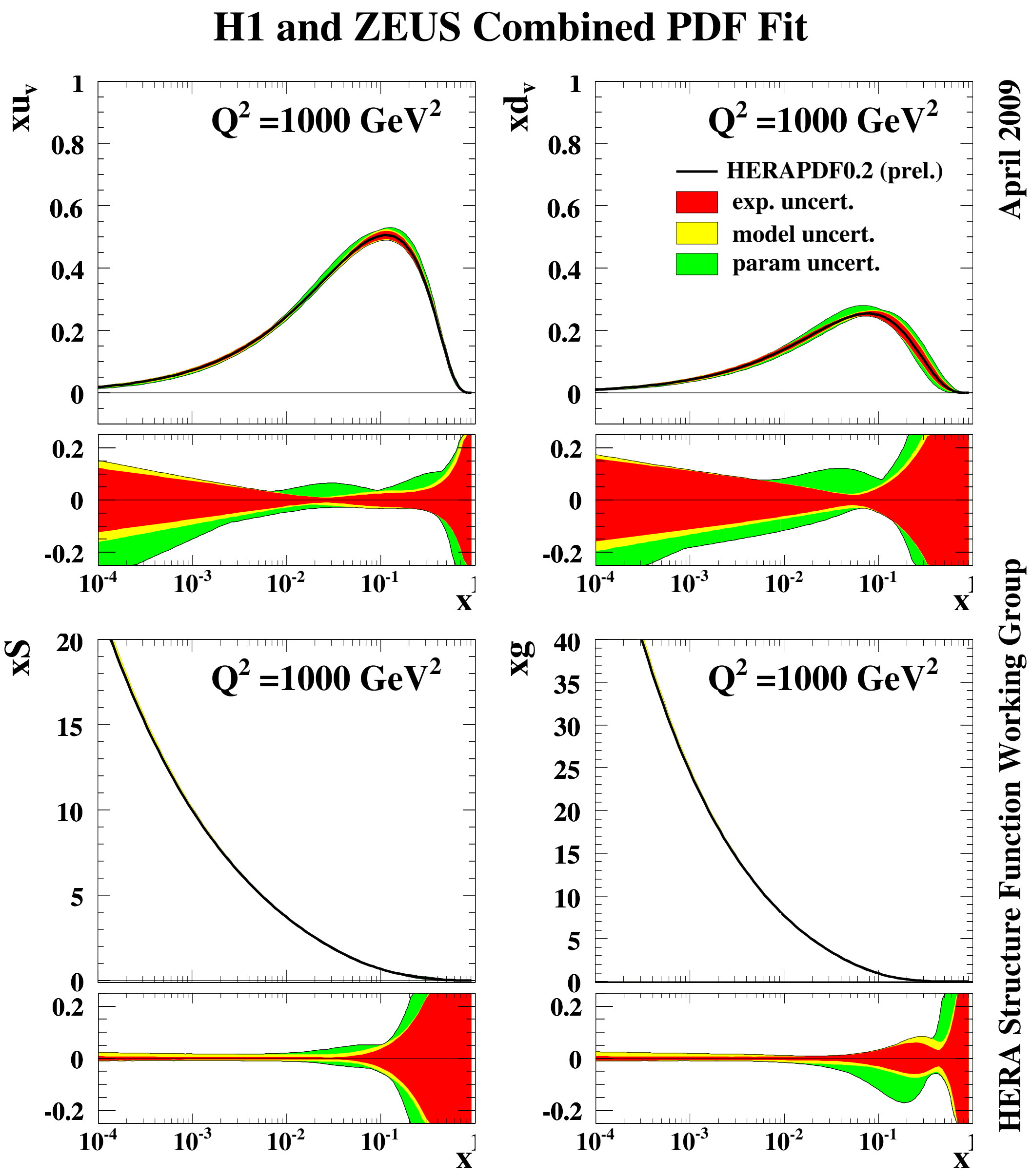

Figure 25: Figure shows the PDF distributions for the xu_v, xd_v, xS, and xg and their relative uncertainties which include the experimental (red), model (yellow), and parametrisation (green) uncertainties at the $Q^2 = 1000$ GeV^2. The HERAPDF0.2 errors of the sea and gluon distributions in the low x region have an impresive precision. The valence distributions are dominated by the parametrisation uncertainties and at high x this unceratinty dominates all the distributions.

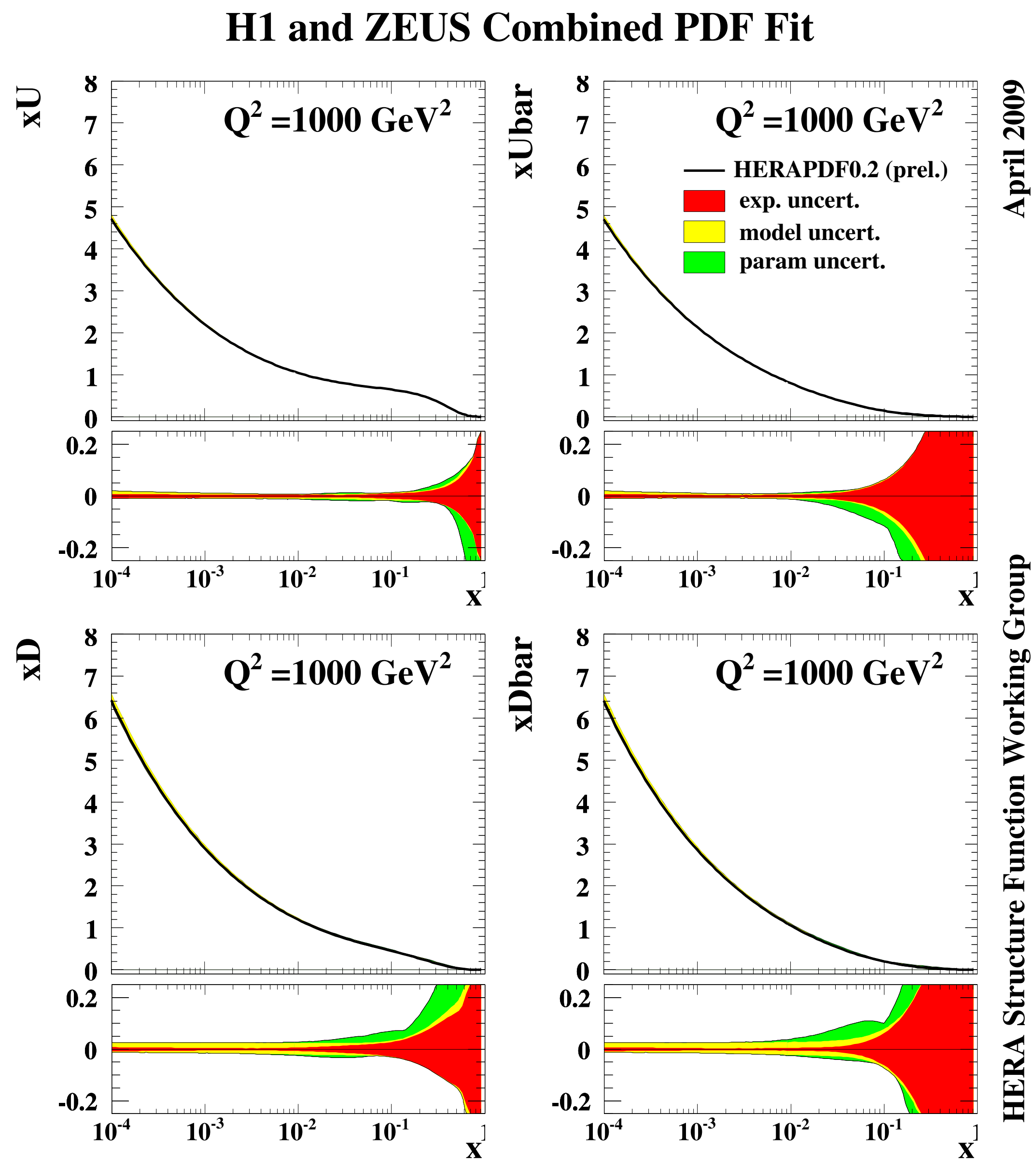

Figure 26: Figure shows the PDF distributions for the xU, $x\bar{U}$, xD, and $x\bar{D}$ and their relative uncertainties which include the experimental (red), model (yellow), and parametrisation (green) uncertainties at the $Q^2 = 1000$ GeV^2. The HERAPDF0.2 errors at this scale are impressive, especially in the low x region. At high x the parametrisation unceratinty dominates.

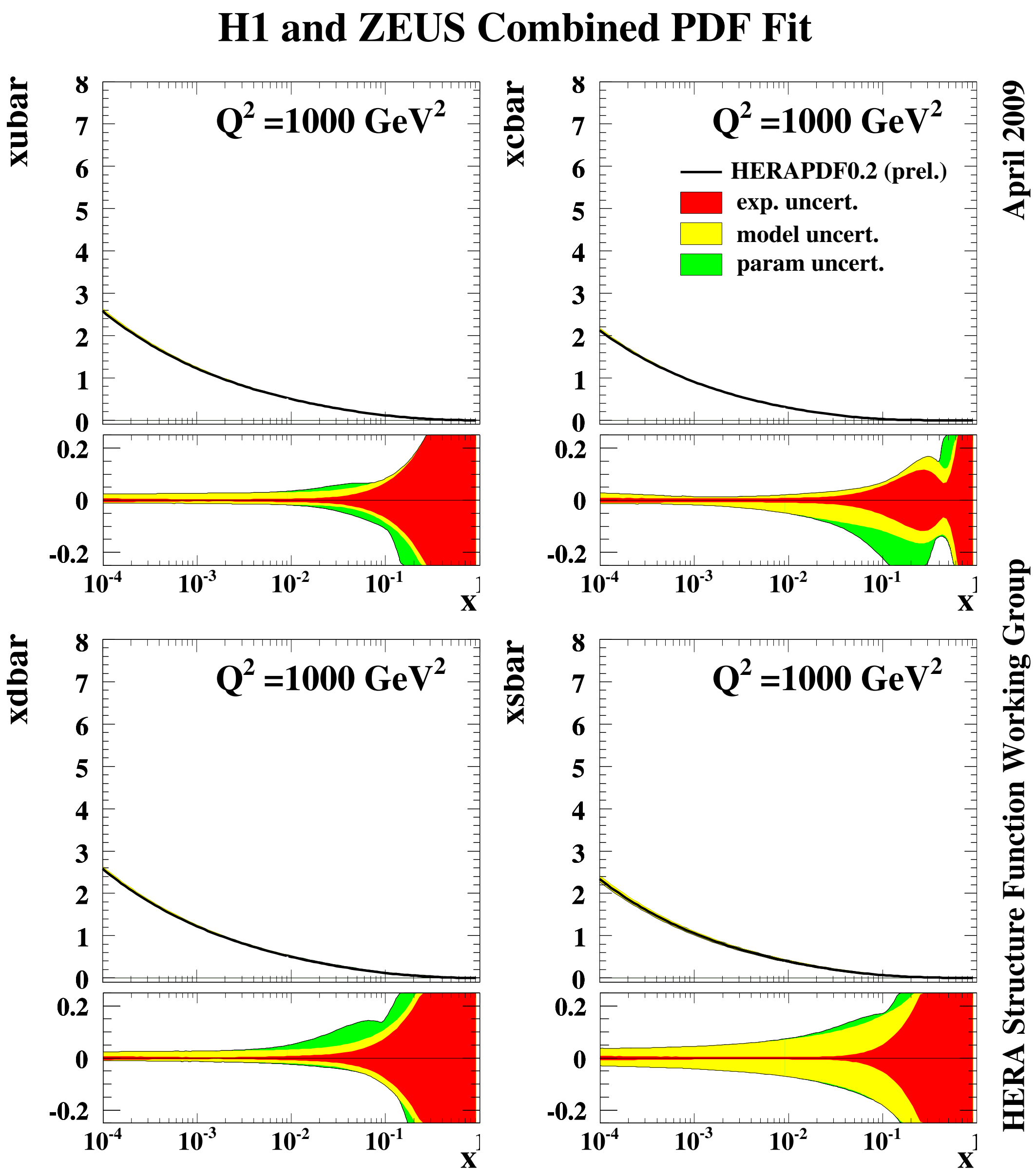

Figure 27: Figure shows the PDF distributions for the $x\bar{u}$, $x\bar{c}$, $x\bar{d}$, and $x\bar{s}$ and their relative uncertainties which include the experimental (red), model (yellow), and parametrisation (green) uncertainties at the $Q^2 = 1000$ GeV^2. The HERAPDF0.2 errors at this scale are impressive, especially in the low x region. At high x the parametrisation unceratinty dominates.

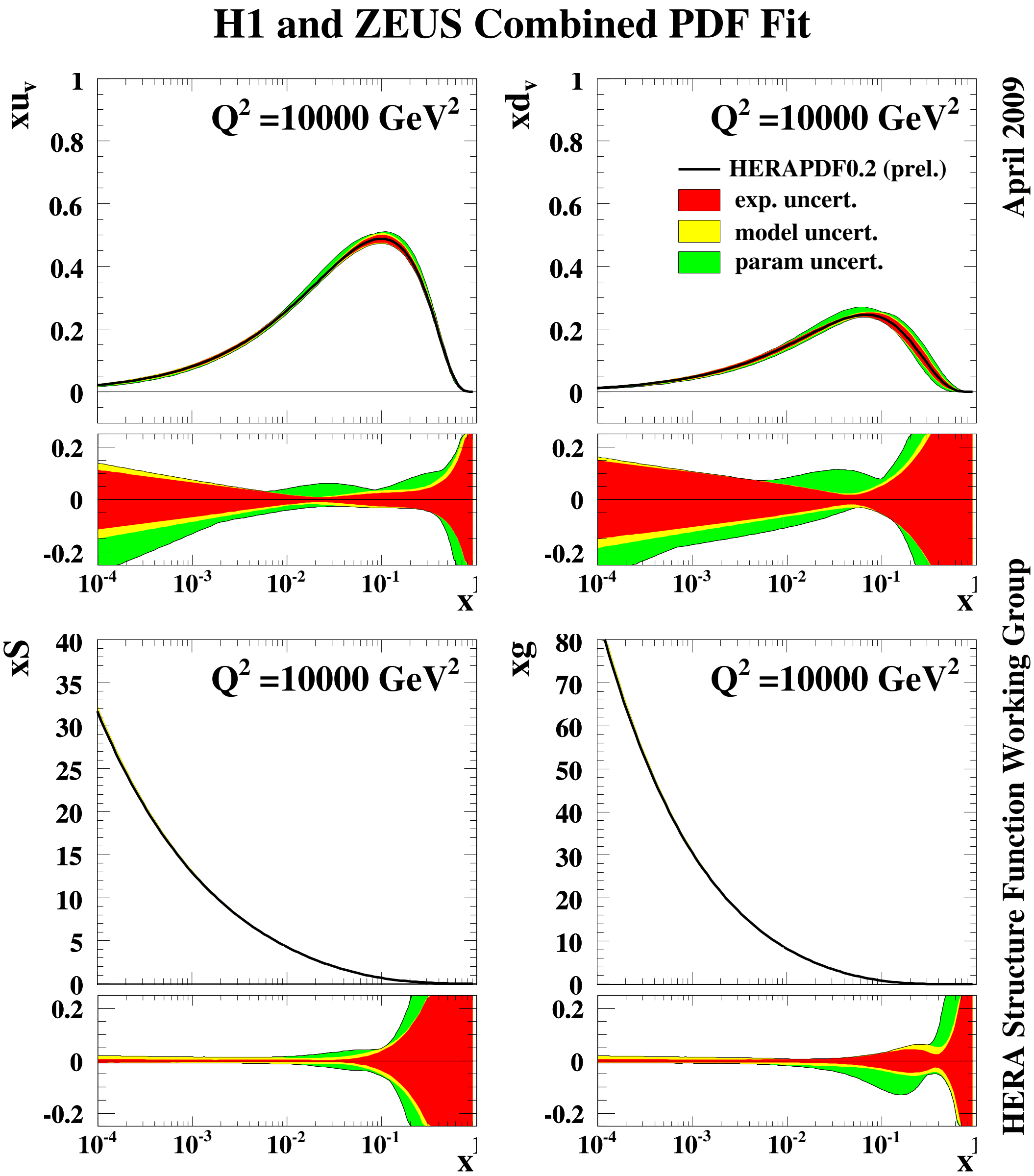

Figure 28: Figure shows the PDF distributions for the xu_v, xd_v, xS, and xg and their relative uncertainties which include the experimental (red), model (yellow), and parametrisation (green) uncertainties at the $Q^2 = 10000$ GeV^2, scale relevant for the LHC. At this scale, the HERAPDF0.2 errors of the sea and gluon distributions in the low x region have an impresive precision. The valence distributions are dominated by the parametrisation uncertainties and at high x this unceratinty dominates all the distributions.

H1 and ZEUS Combined PDF Fit

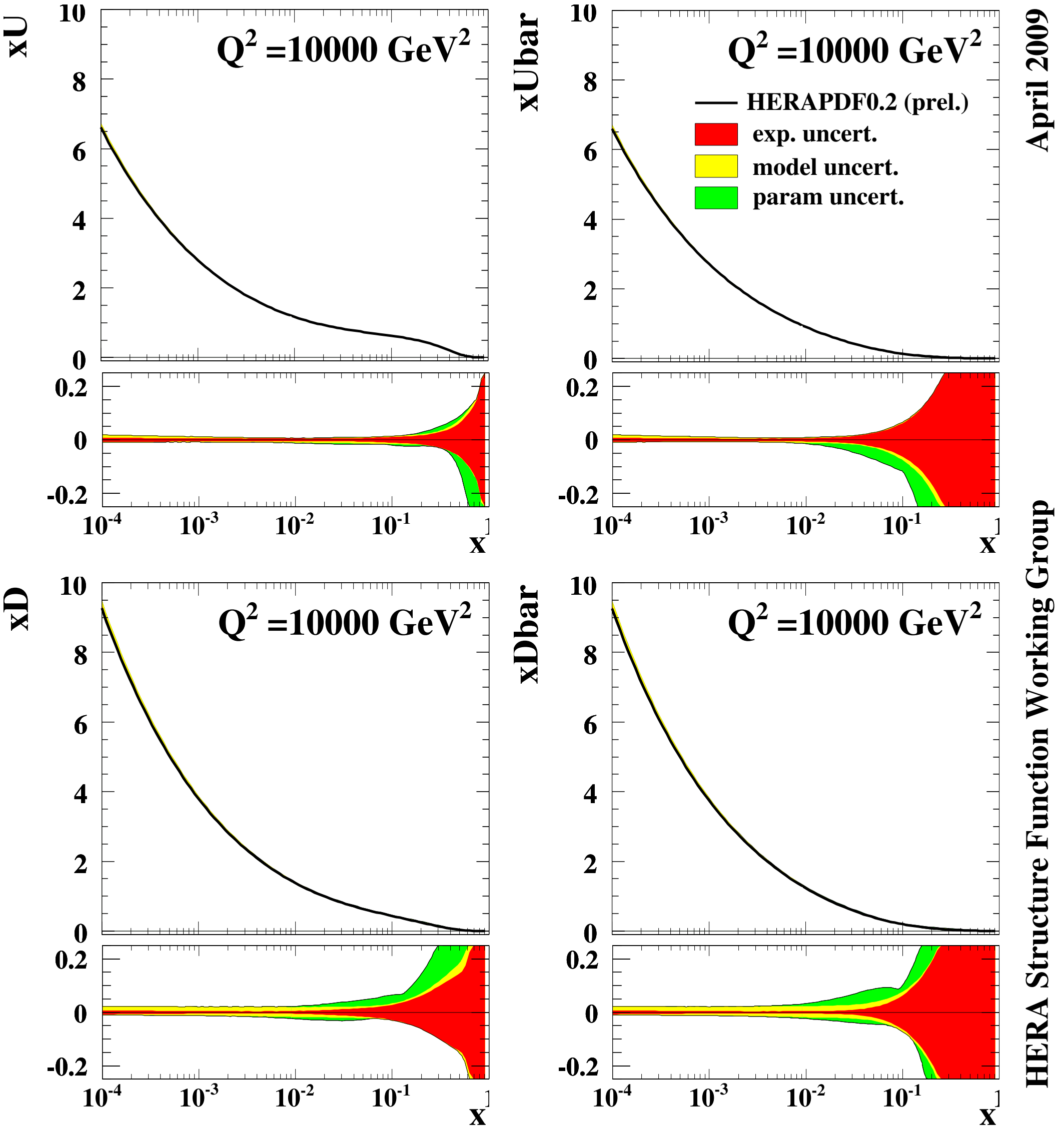

Figure 29: Figure shows the PDF distributions for the xU, $x\bar{U}$, xD, and $x\bar{D}$ and their relative uncertainties which include the experimental (red), model (yellow), and parametrisation (green) uncertainties at the $Q^2 = 10000$ GeV^2, scale relevant for the LHC. The HERAPDF0.2 errors at this scale are impressive, especially in the low x region. At high x the parametrisation unceratinty dominates.

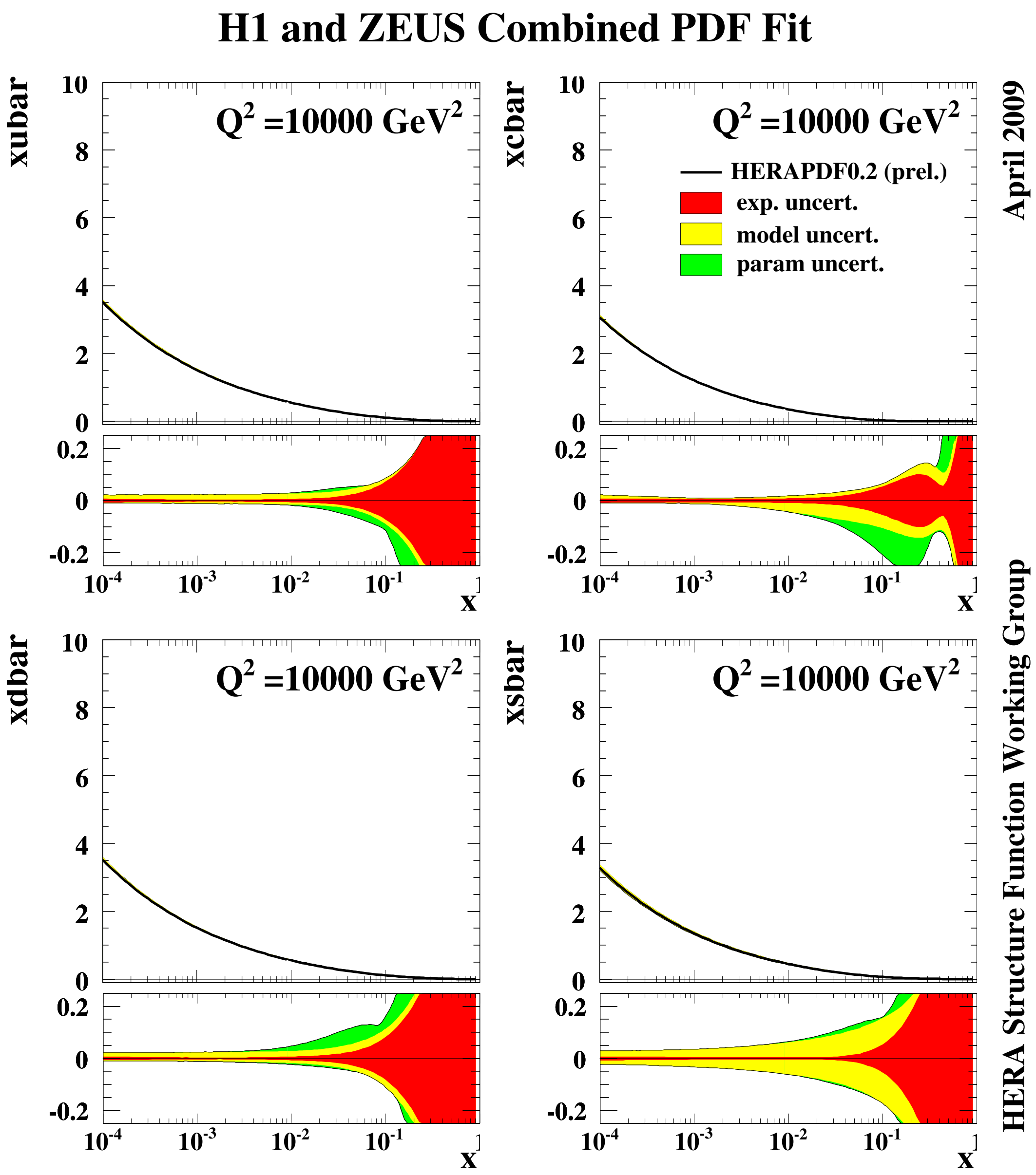

Figure 30: Figure shows the PDF distributions for the $x\bar{u}$, $x\bar{c}$, $x\bar{d}$, and $x\bar{s}$ and their relative uncertainties which include the experimental (red), model (yellow), and parametrisation (green) uncertainties at the $Q^2 = 10000$ GeV^2, scale relevant for the LHC. The HERAPDF0.2 errors at this scale are impressive, especially in the low x region. At high x the parametrisation uncertainty dominates.

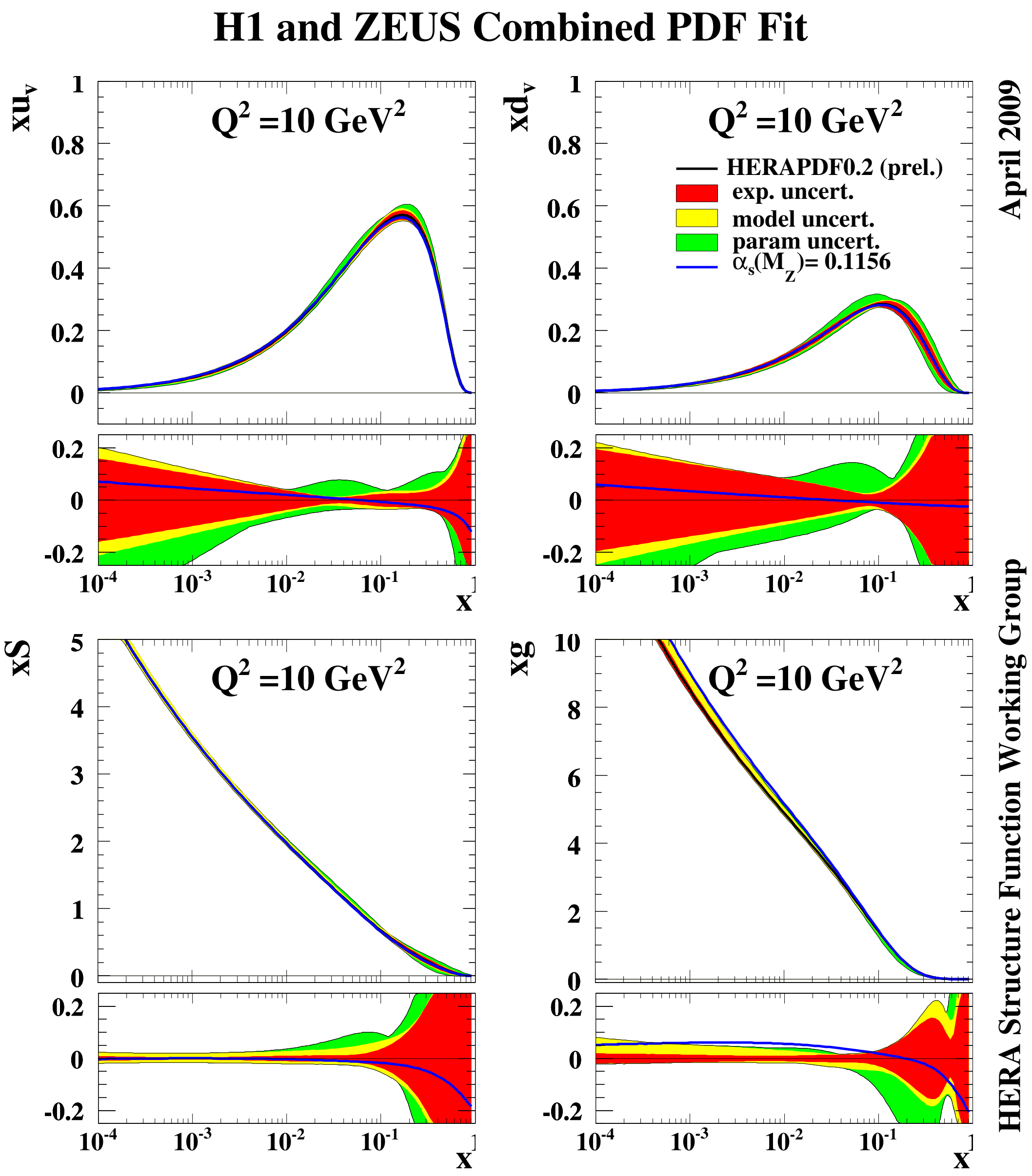

Figure 31: Figure shows the effect of variation of α_S to its lower bound limit of 0.1156 for the world average range of the $\alpha_S(M_Z)$ on the PDF distributions xu_v, xd_v, xS and xg at a scale of $Q^2 = 10$ GeV^2. The effect is better observed when the relative uncertainties are shown, the blue line marks the size of the effect of varying the $\alpha_S(M_Z) = 0.1156$. As expected, the most affected distribution is that of the gluon as there is a strong correlation between them.

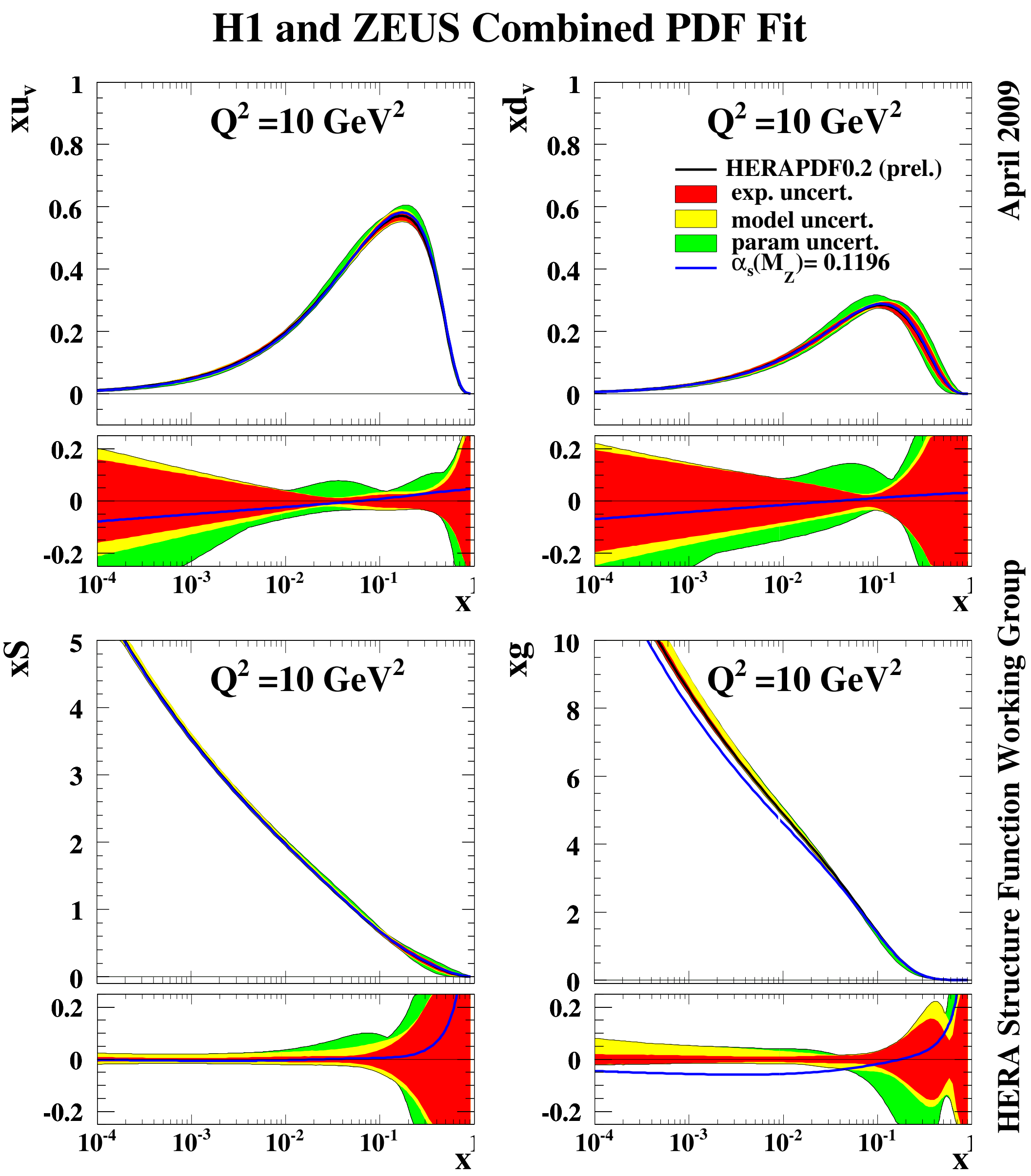

Figure 32: Figure shows the effect of variation of α_S to its upper bound limit of 0.1196 for the world average range of the $\alpha_S(M_Z)$ on the PDF distributions xu_v, xd_v, xS and xg at a scale of $Q^2 = 10$ GeV^2. The effect is better observed when the relative uncertainties are shown, the blue line marks the size of the effect of varying the $\alpha_S(M_Z) = 0.1196$. As expected, the most affected distribution is that of the gluon as there is a strong correlation between them.

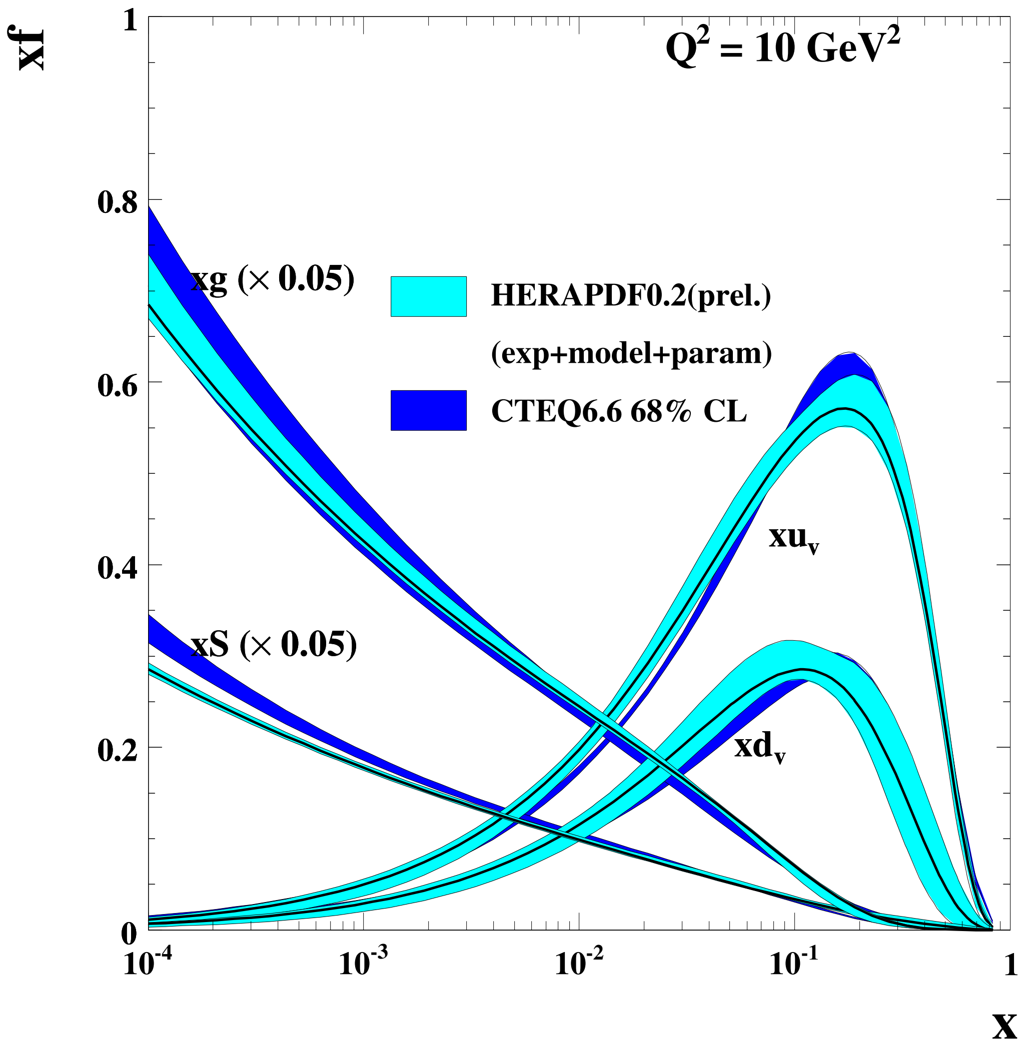

Figure 33: Figure shows the comparison between the CTEQ6.6 (blue) and HERAPDF0.2 (cyan) sets of PDFs at $Q^2 = 10$ GeV^2. The CTEQ6.6 PDF distributions are shown at 68% Confidence Level (CL). The HERAPDF0.2 error band includes the experimental, model and parametrisation uncertainties. The PDF sets shown are the gluon, sea, and valence distributions for up and down quarks.

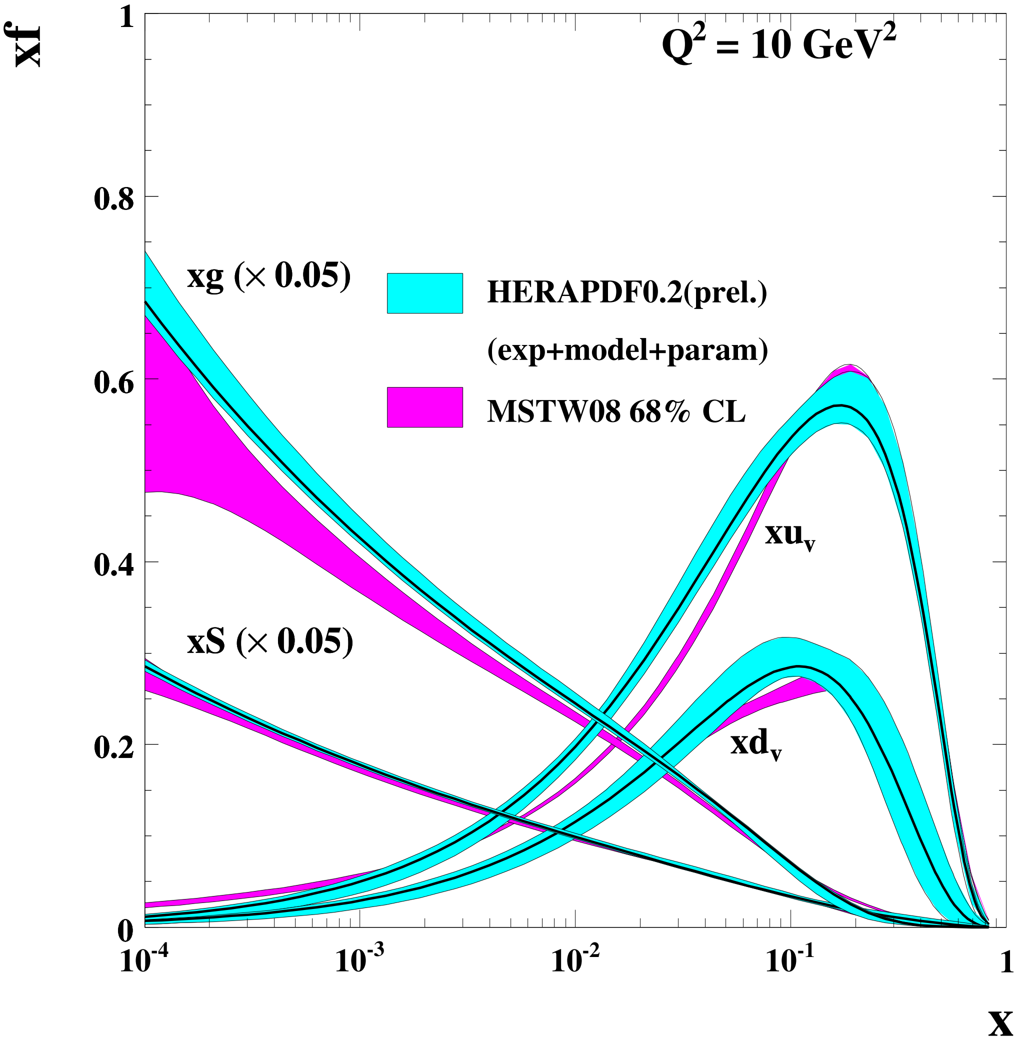

Figure 34: Figure shows the comparison between the MSTW08 (magenta) and HERAPDF0.2 (cyan) sets of PDFs at $Q^2 = 10$ GeV^2. The MSTW08 PDF distributions are shown at 68% Confidence Level (CL). The HERAPDF0.2 error band includes the experimental, model and parametrisation uncertainties. The PDF sets shown are the gluon, sea, and valence distributions for up and down quarks.

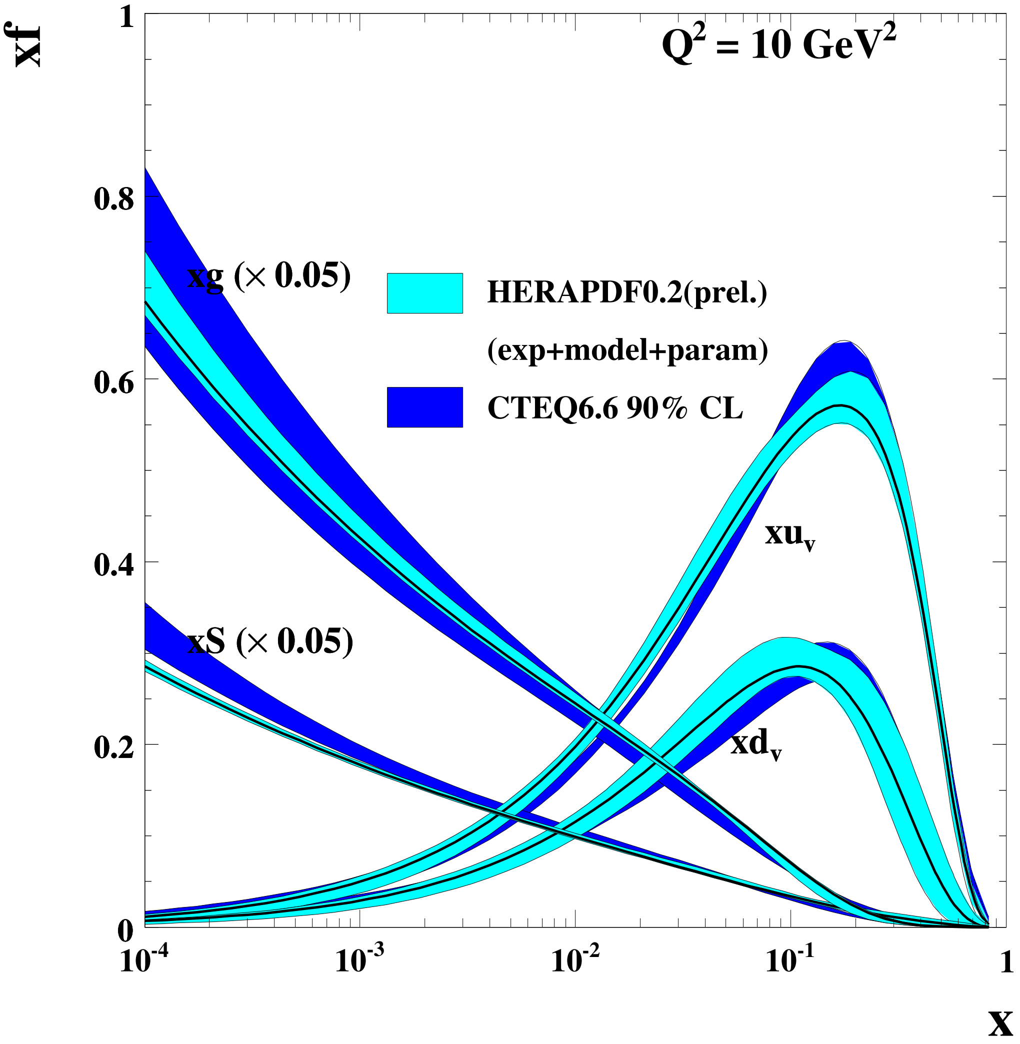

Figure 35: Figure shows the comparison between the CTEQ6.6 (blue) and HERAPDF0.2 (cyan) sets of PDFs at $Q^2 = 10$ GeV^2. The CTEQ6.6 PDF distributions are shown at 90% Confidence Level (CL). The HERAPDF0.2 error band includes the experimental, model and parametrisation uncertainties. The PDF sets shown are the gluon, sea, and valence distributions for up and down quarks.

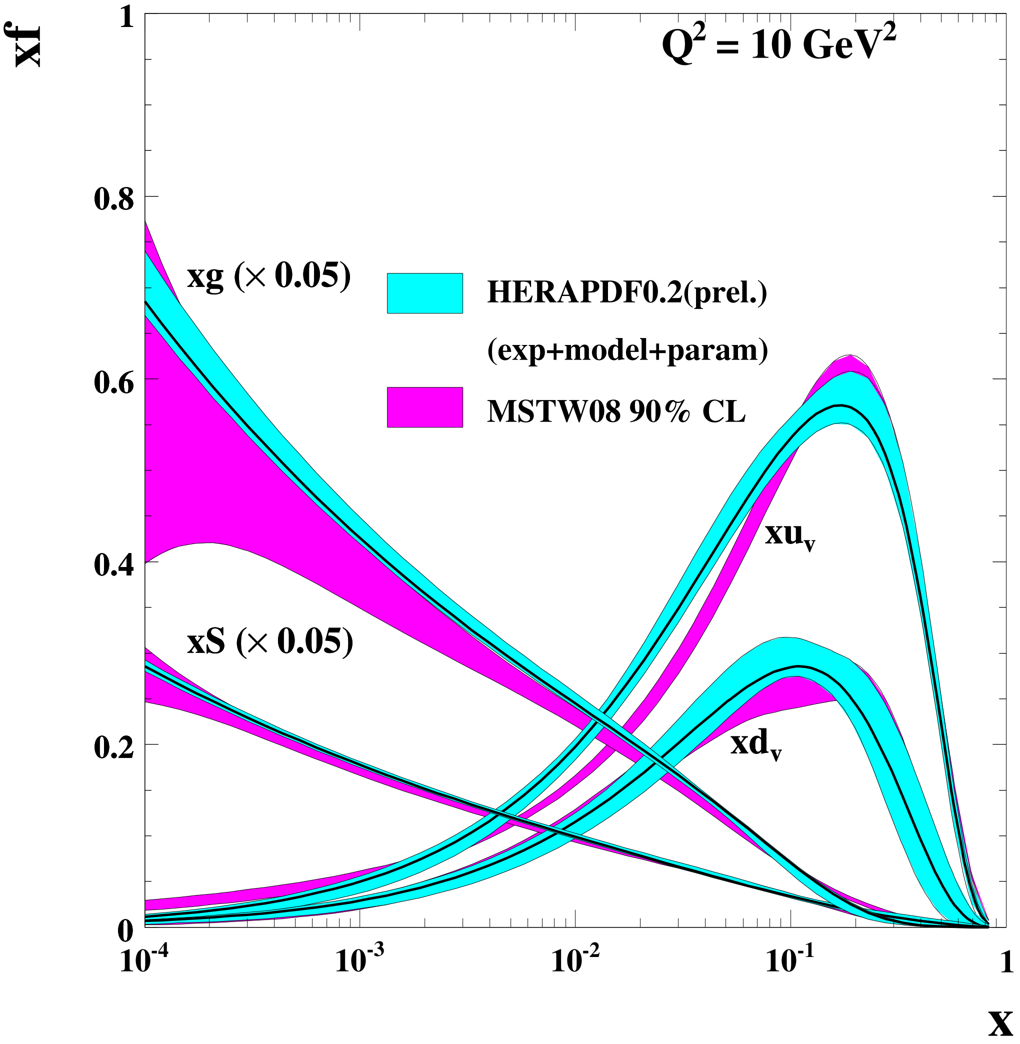

Figure 36: Figure shows the comparison between the MSTW08 (magenta) and HERAPDF0.2 (cyan) sets of PDFs at $Q^2 = 10$ GeV^2. The MSTW08 PDF distributions are shown at 90% Confidence Level (CL). The HERAPDF0.2 error band includes the experimental, model and parametrisation uncertainties. The PDF sets shown are the gluon, sea, and valence distributions for up and down quarks.